A decade (2008-2017) of water stable-isotope composition of precipitation at Concordia Station, East Antarctica

Giuliano Dreossi[1,2], Mauro Masiol[1], Barbara Stenni[1], Daniele Zannoni[1], Claudio Scarchilli[3], Virginia Ciardini[3], Mathieu Casado[4], Amaëlle Landais[4], Martin Werner[5], Alexandre Cauquoin[6], Giampietro Casasanta[7], Massimo Del Guasta[8], Vittoria Posocco[1], and Carlo Barbante[2]

1. Department of Environmental Sciences, Informatics and Statistics, Ca' Foscari University of Venice, Mestre Venice, Italy
2. Institute of Polar Sciences, National Research Council of Italy (ISP-CNR), Mestre Venice, Italy
3. ENEA, Laboratory for Observations and Measures for the Environment and Climate, Rome, 00123, Italy
4. Laboratoire des Sciences du Climat et de l'Environnement, LSCE/IPSL, CEA-CNRS-UVSQ, Université Paris-Saclay, Gif sur Yvette, France
5. Alfred Wegener Institute (AWI), Helmholtz Centre for Polar and Marine Research, Bremerhaven, Germany
6. Institute of Industrial Science, The University of Tokyo, Kashiwa, Japan
7. Institute of Atmospheric Sciences and Climate, National Research Council of Italy (INO-CNR), Bologna, Italy
8. National Institute of Optics, National Research Council of Italy (INO-CNR), Sesto Fiorentino (FI), Italy

Correspondence to: Mauro Masiol (mauro.masiol@unive.it) and Barbara Stenni (barbara.stenni@unive.it)

Abstract. A ten-year record of oxygen and hydrogen isotopic composition of precipitation is here presented: from 2008 to 2017, 1483 daily precipitation samples were collected all-year round on a raised platform at Concordia Station, East Antarctica. Weather data were retrieved from the Italian Antarctic Meteo-Climatological Observatory Automatic Weather Station (AWS), while ERA5 was used to estimate total precipitation. The δ-temperature relationships were moderately high for daily data (r^2=0.63 and 0.64 for $\delta^{18}O$ and δ^2H, respectively) and stronger using monthly data (r^2=0.82 for both $\delta^{18}O$ and δ^2H), with a slope of about 0.5‰/°C for $\delta^{18}O/T_{AWS}$ (3.5 ‰/°C for δ^2H/T_{AWS}), which remains consistent also using annual averages. The isotopic composition of precipitation is the input signal of the snow/ice system and this dataset will be useful to improve the interpretation of paleoclimate records and promote a better understanding of the post-depositional processes affecting the isotopic signal in ice cores. This dataset represents a benchmark for the evaluation of isotope-enabled general

circulation models. Here, the ECHAM6-wiso output were compared to experimental data, showing moderately good relationships for $\delta^{18}O$ and $\delta^{2}H$, but not for d-excess, nonetheless marking a substantial improvement from the previous release of the model.

1 Introduction

Throughout the hydrological cycle, air masses undergo evaporation, condensation, and successive precipitation events, during which temperature-dependent exchanges of heavy and light isotopes happen due to their slightly different microphysical properties. These processes drive the variation of the isotopic composition of water through all stages of the hydrological cycle and among different reservoirs, e.g., the atmosphere, oceans, superficial waters, groundwaters, and the cryosphere (e.g., Dansgaard, 1964; Rozanski et al., 1993; Jouzel, 2014). Consequently, ratios among the three stable isotopes of oxygen (^{16}O, ^{17}O, ^{18}O) and the two of hydrogen (^{1}H, ^{2}H) have been extensively used as proxies for hydrological, ecohydrological, climatological, palaeoclimatological, environmental, and agricultural studies from local to global scales (Yoshimura, 2015). Oxygen and hydrogen isotope ratios are commonly reported as deviations relative to an international standard and are expressed in per mil (‰):

$$\delta = \frac{R_X - R_{std}}{R_{std}} 10^3 \quad (1)$$

where R_X is either the $^{18}O/^{16}O$ or $^{2}H/^{1}H$ ratio in the sample and R_{std} is the same ratio in the V-SMOW standard (Vienna Standard Mean Ocean Water).

The local temperature at the precipitation site is recognized as the main factor driving the isotopic composition of precipitation. Since the 1950s, a robust relationship between the annual values of the isotopic composition of precipitations and the average annual local air temperature was reported in mid and high latitudes (Dansgaard 1953; Epstein and Mayeda 1953; Craig 1961; Dansgaard, 1964; Jouzel et al., 1997, 2003). In polar regions, this relationship was further supported by theoretical distillation models (Jouzel and Merlivat, 1984) and atmospheric general circulation models (GCMs) (e.g., Risi et al., 2010; Werner et al., 2011).

Besides delta values, the second order parameter deuterium excess ($d=\delta^{2}H-8\cdot\delta^{18}O$; Dansgaard, 1964) provides additional information on the evaporation conditions at precipitation source regions, i.e., the humidity relative to saturation during evaporation, the sea surface temperature and, to a limited extent, the wind speed (Merlivat and Jouzel, 1979; Uemura et al., 2008; Pfahl and Sodemann, 2014; Zannoni et al., 2022). A positive (>0) d-excess is driven by the higher diffusivity of $^{2}H^{1}H^{16}O$ related to $^{1}H^{1}H^{18}O$; the result is a relative enrichment of $^{2}H^{1}H^{16}O$ in

the vapor-phase during the evaporation process if there is not sufficient time for achieving the isotopic equilibrium between the two phases.

The isotopic composition of surface snow was extensively analyzed in Antarctica, mostly along traverses or close to inland stations. Masson-Delmotte et al. (2008) summarized the available data on the isotopic composition of surface snow across the Antarctic continent. Firn temperature is also usually measured together with snow sample collection as an indicator of mean annual surface temperature (Epstein et al., 1963). These data are extremely important for paleoclimatology: assuming the empirical δ-T relationship is valid over time at a specific location, the isotope-temperature slope can be used as an "isotopic thermometer", i.e., to quantify past temperature changes based on the stable isotopic composition. Following this approach, water stable-isotope geochemistry has been widely applied to polar paleoclimate research. The past Earth's climate was reconstructed for over half a century using this approach applied to stratigraphic records of water in ice and firn cores (e.g., Langway, 1958; Gonfiantini and Picciotto, 1959; Dansgaard et al., 1969; Dansgaard et al., 1993; EPICA Community Members, 2004; Jouzel et al., 2007; Jouzel, 2014; Stenni et al., 2017).

In East Antarctica, where snow accumulation rates are sufficiently low, several deep ice cores recovered over the last decades have provided the reconstructions of past climatic cycles, e.g., 343 kyr (thousands of years) at Talos Dome (Crotti et al., 2021), 420 kyr at Vostok (Petit et al., 1999), 720 kyr at Dome Fuji (Kawamura et al., 2017) and 800 kyr at EPICA Dome C (EPICA community members, 2004; Jouzel et al., 2007). Currently, the European project "Beyond EPICA oldest ice" is underway in the location known as Little Dome C (approx. 35 km from Dome C), aiming to obtain quantitative and high-resolution ice-core information on climate and environmental changes up to 1.5 Myr (Parrenin et al., 2017).

Major limitations undermine the use of water isotopes for the reconstruction of past temperatures and may bias the interpretation of the paleoclimate records. First, the low snow accumulation rates in inland Antarctica, in combination with wind redistribution effects and stratigraphic noise not related to climate, allow only lower temporal resolutions of ice-core reconstructions compared to high accumulation of coastal regions, generally not finer than decadal or even multidecadal (Petit et al., 1982; Ekaykin et al., 2002; 2004; Frezzotti et al., 2007; Münch et al., 2016; Casado et al., 2018). Another major challenge is linked to the ways the isotopic signal is imprinted and preserved in ice and firn, which is not only shaped by the sensitivity to condensation temperature but also includes further signals of various processes with potentially significant effects on the isotopic fractionation (Casado et al., 2020; 2021). The processes recognized to affect the fractionation processes and mixing during and after the deposition of precipitations were reviewed by Casado et al. (2018) and Ma et al. (2020) and include: (i) processes within the local boundary layer leading to non-constant relationships between the isotopic composition

of snow and surface temperature over time and space (Krinner et al., 1997), (ii) variations in air mass transport trajectories through time (Delaygue et al., 2000; Schlosser et al., 2004), (iii) evaporation conditions at the source of moisture (Vimeux et al., 1999), (iv) sea surface boundary conditions (Cauquoin et al., 2023); (v) seasonal variations and intermittency of precipitation and accumulation (Touzeau et al., 2016; Casado et al., 2020); (vi) redistribution of snow by surface winds (Groot Zwaaftink et al., 2013; Picard et al., 2019), (vii) water vapor exchanges between surface snow and the atmosphere due to sublimation and solid condensation (Ritter et al., 2016; Genthon et al., 2017); (viii) surface snow metamorphism (Picard et al., 2012; Casado et al., 2021) and (ix) isotopic diffusion within the firn (Laepple et al., 2018).

These post-depositional processes are expected to account for large uncertainties in low-accumulation areas, such as East Antarctica, where (i) there is a low precipitation rate (Bromwich et al., 2004; Palerme et al., 2017; Scarchilli et al., 2011; Casado et al., 2018; 2020), (ii) the atmospheric dynamics and pathways and surface mass balance (SMB) are yet to be fully understood (Frezzotti et al., 2004; 2007; Urbini et al., 2008; Scarchilli et al., 2010; 2011), and (iii) the snow surface remains exposed to the atmosphere for a long time, allowing prolonged interactions and exchanges at the snow-atmosphere interface, longer mixing and potential horizontal transports by winds. Although all these processes are potentially able to bias the pristine isotopic signal of precipitation, their effects on driving the isotopic composition of Antarctic precipitation are still unclear and have not yet been fully quantified. Consequently, the different sensitivity of the empirical δ-T relationship in East Antarctic ice is generally poorly constrained (Sime et al., 2009; Stenni et al., 2017; Münch et al., 2016). Because of these limitations, a nonconstant relationship between the snow isotopic composition and air temperature through time and space is expected, as already evidenced by Masson-Delmotte et al. (2008). Other studies further suggest that the δ-T in East Antarctica may vary among ice core sites, with the climatic signal expected to account for only 10%–50% of the variance in $\delta^{18}O$ (Münch and Laepple, 2018; Laepple et al., 2018; Casado et al., 2020; 2021). The three years monitoring (Jan 2008-Dec 2010) of daily precipitation collected at the Concordia Station in the East Antarctic plateau showed clear relationships between the isotopic composition and local air temperature at daily (R^2=0.63) and monthly (R^2=0.82) scales (Stenni et al., 2016). However, the temporal relationship between daily $\delta^{18}O$ and air temperature was approximately 2-folds smaller than the average Antarctic spatial relationship obtained by Masson-Delmotte et al. (2008), i.e., the one used for the interpretation of the EPICA Dome C record (0.49‰/°C vs. 0.8‰/°C). Hence, the slopes between the delta values and temperature have been shown to be highly variable considering different time intervals and locations (Casado et al., 2017). On the contrary, by reconstructing the magnitude of the last glacial maximum cooling using borehole thermometry, Buizert et al. (2021) showed a large variability of the δ-temperature slope considering different ice core locations. Generally,

this latter study reported quite higher δ-T slopes (range 0.82-1.45 ‰/°C) than studies using water isotope composition. This represents a long-lasting, controversial, and still unsolved question in paleoclimate reconstructions from Antarctic ice cores.

Under this view, there is a need for a better understanding of how the isotopic composition of water is imprinted in the fresh snow and firn and how it evolves to obtain robust and unbiased empirical relationships between climate and stable water isotope signatures. Since the preliminary study by Stenni et al. (2016), the precipitation collection at Concordia Station for analyzing the isotopic composition has continued until the present day and it is still ongoing. Here, results spanning over 10 years (2008-2017) are reported and discussed. This dataset represents an unprecedentedly long record of precipitation experimentally measured in East Antarctica with several potential advantages for glaciological and palaeoclimatological studies:

- a better framing of the inter-annual variability of the isotopic composition of precipitation with respect to previous works. Indeed, 10 years of observations more likely include atmospheric processes acting on scales larger than 3 years;
- a more robust evaluation of the state-of-the-art isotope-enabled general circulation models (iGCMs) performances thanks to comparisons of 10 year-long experimental data with outputs from different iGCMs. For instance, the data provided in the present study may help to improve cloud parameterization through d-excess model-data comparisons (e.g., microphysics scheme, ice nucleation rates);
- experimentally collected precipitation data can be used as input of isotopic models investigating post-depositional processes of surface snow, firn, and ice core records, since the precipitation isotopic composition is the input signal of the atmosphere-snow surface and subsurface systems;
- the basic statistical results, e.g., meteoric water lines, seasonal patterns, weighted values, etc., presented in this study are scaled over different periods, such as daily, monthly, inter-annual scales. These data may therefore be useful to researchers working on different scientific areas, such as atmosphere, climate and weather. For instance, the data provided in this study may be useful to better constrain the δ-T thermometer. To this end, the data used in this study are presented as both weighted and unweighted for precipitation amounts. For example, such temporally high-resolved data are necessary to better understand and evaluate the impact of extreme snowfall events on the precipitation-weighted $\delta^{18}O$-temperature relationship in both observed and modeled isotope data.

2 Materials and methods

2.1 Precipitation collection

Concordia Station (75°06'S, 123°21'E; elevation 3233 m a.s.l.) is a French–Italian research facility located at Dome C on the East Antarctic Plateau (Figure S1, http://www.concordiastation.aq) open all year round since 2005. The sampling site is located in a clean area, approx. 800 m from the station, to avoid contamination from the anthropogenic operations. Precipitation accumulates over an 80x120 cm wooden platform standing 1 m above the snow surface. The platform is covered by a polystyrene/polytetrafluoroethylene surface and is shielded by an 8-cm rail to prevent snow from being blown off from the surface. Samples were manually collected with daily frequency by removing all the accumulated material, which was immediately sealed into labelled plastic bags. Bags were preserved in a frozen state until the analysis. If no snow or a too low amount of snow was found on the plate, no sample was collected, and the plate was cleaned. The amount of deposited snow varied depending on the amount of precipitation from 0 to ~10 mm, with isolated cases of 30–50 mm deposition possibly related to blowing snow events. The sample is therefore representative of a fresh snowfall, but it may also include snow blown onto or off the platform by winds. Every day, the collection of the samples was recorded in a logbook reporting the timing and some weather variables. Generally, the sample collection occurred in the morning between 9 am and noon, local time (UTC+8) and when meteorological conditions do not put at risk the personnel' safety.

2.2 Water stable isotopes analysis of precipitation samples

Once in the lab, samples were melted at room temperature, transferred into 25 mL high-density polyethylene capped bottles, and then stored at -20°C until analysis. The isotopic composition ($\delta^{18}O$ and $\delta^{2}H$) of the samples was determined by the well-established CO_2-H_2/water equilibration method adapted from Epstein and Mayeda (1953) and Horita (1988), followed by isotope ratio mass spectrometry (IRMS) analysis. IRMS was composed of a Thermo-Fisher Delta Plus Advantage mass spectrometer coupled with an automatic equilibration device (Finnigan MAT HDO 1086).

Since IRMS requires at least 4 mL water volume, smaller samples of melted snow were directly analyzed without any pre-processing by cavity ring-down spectroscopy (CRDS). CRDS analysis was performed with PICARRO model L1102-*i* and model L2130-*i* equipped with a A1102 vaporizer device. Between-sample memory effects may bias CRDS analyses (Penna et al., 2012), therefore samples were injected 8 times and results were filtered using an outlier test, i.e., discarding all the results falling outside of the interval described by the average of the 8 repetitions ± standard deviation.

All data were expressed as relative to the international standard VSMOW. Two working standards were used during each run to build the calibration line and a third working standard was used for quality control. All the working standards are in the range of very negative values as found in Antarctic snow and were regularly calibrated against VSMOW-SLAP. Internal laboratory tests have shown the linearity of the instrumental response outside of the calibration interval. Data consistency between analytical methods was assured by several laboratory tests carried out to detect possible biases due to the use of IRMS or CRDS. Average differences were in the order of analytical precision of IRMS (better or equal to ±0.05‰ for $\delta^{18}O$ and ±0.7‰ for $\delta^{2}H$) and the analytical precision for CRDS (±0.10‰ for $\delta^{18}O$ and ±0.5‰ for $\delta^{2}H$).

2.3 Weather observations and reanalysis data

Weather data measured at Concordia Station were retrieved from the automatic weather station (AWS) Concordia (WMO ID: 89625), managed by the Italian Antarctic Meteo-Climatological Observatory (Grigioni et al., 2022a) and operating since 2005. AWS data include air temperature (T_{AWS}, °C), pressure ($Press_{AWS}$, hPa), relative humidity (RH_{AWS}, %), wind speed (ws_{AWS}, m s^{-1}) and direction (wd_{AWS}, degrees). Missing hourly AWS data (8.5 %) were reconstructed through linear regression using data measured at the nearby AWS "Dome C II" (WMO ID: 89828), an American station installed in 1995 by the Antarctic Meteorological Research Center (AMRC). The coefficient of determination between AWSs was r^2=0.99 for air temperature and surface pressure, r^2=0.70 for wind speed. Surface-based temperature inversions (SBTIs) frequently occur within the atmospheric boundary layer across continental Antarctica (Connolley, 1996; Pietroni et al., 2014). At Concordia, strong and long-lived SBTIs are generally observed, reaching up to 40°C in winter and mostly extending within the lowest 100 m of height, while they may disappear only in the early afternoon during summer due to maximum insolation and convective mixing (Genthon et al., 2010; Argentini et al., 2014; Petenko et al., 2019). Since the condensation temperature can be approximated to the temperature at the upper limit of the inversion layer (Masson-Delmotte et al., 2008), data from daily radiosounding profiles were processed to determine the temperature at the bottom of the first layer where temperature decreases with altitude (T_{INV}). The inversion strength (I) was calculated as the difference between T_{INV} and T_{AWS} (Connolley, 1996). Data of solar direct radiation (Direct rad_{BSRN}, W m^{-2}) measured at Concordia station were retrieved from the Baseline Surface Radiation Network (BSRN), a network of the Work Climate Research Program (WCRP) (Ohmura et al., 1998; Driemel et al., 2018; Lupi et al., 2021; Bai et al., 2022).

Reanalysis meteorological data were retrieved from the European Centre for Medium-Range Weather Forecasts (ECMWF) ERA5 (Hersbach et al., 2023); data of 2 m temperature ($T_{2m\ ERA5}$), surface pressure ($Press_{ERA5}$), total

precipitation (tp_{ERA5}), evaporation (e_{ERA5}), cloud base height data (cbh_{ERA5}) were downloaded from the Copernicus Climate Change Service (C3S) Climate Data Store (CDS). Relative humidity (RH_{ERA5}) was computed from vapor pressure and saturation vapor pressure according to the Murphy and Koop (2005) formulae and using hourly ERA5 data.

The AWSs, BSRN and ERA5 provide meteorological variables with different frequencies (minutes to hours); daily averages were calculated either relative to the local time for investigating the daily patterns or relative to the exact extension of the sampling time for the fine match with the isotopic composition of precipitation, i.e., referring to the information in the logbook. Since missing data can affect the analysis, daily averages were computed only for days having at least 75% of the available hourly records; monthly averages/medians for months having at least 75% of the available days. When used along with the isotopic composition of snow, monthly and annual-averaged weather data were computed only over days with available samples. Given the qualitative nature of the observed accumulation, the tp_{ERA5} parameter has been used in this study as representative of the precipitation amount of the observed daily snow samples.

The Southern Annular Mode (SAM, aka Antarctic Oscillation, AAO) depicts changes in the position and strength of the westerly wind belt over the Southern Ocean and is defined as the zonal mean atmospheric pressure difference between the mid-latitudes (~40° S) and Antarctica (~65° S) (Thompson and Wallace, 2000; Marshall, 2003). SAM is the predominant atmospheric variability mode in the Southern Hemisphere having important impacts on temperature and precipitation, including in Antarctica (Fogt and Marshall, 2020). Positive SAM phases lead to cool and dry conditions across the continental Antarctic continent and warm and wet conditions over the Antarctic Peninsula. Daily and monthly SAM indexes were retrieved from the Climate Prediction Center, National Centers for Environmental Prediction of NOAA.

In this study, four meteorological seasons are used: Austral summer (December, January, and February [DJF]), autumn (March, April, and May [MAM]), winter (June, July, August [JJA]), and spring (September, October, November [SON]).

2.4 Isotope-enabled general circulation models (ECHAM5-wiso and ECHAM6-wiso)

Since 1980s, several iGCMs have been developed with explicit diagnostics for the isotopic composition of water, e.g., NASA GISS, ECHAM-wiso, GENESIS, LMDZ-iso, iCAM5, MIROC5-iso (Joussaume et al., 1984; Jouzel et al., 1987; Hoffmann et al., 1998; Mathieu et al., 2002; Schmidt et al., 2005, Risi et al., 2010; Nusbaumer et al., 2017; Okazaki and Yoshimura, 2019). By incorporating physical processes influencing the isotopic composition

of all water bodies at all stages of the water cycle, iGCMs return the isotopic composition in precipitation, water vapor, and snow/ice.

ECHAM5-wiso (Werner et al., 2011) and ECHAM6-wiso (Cauquoin et al., 2019; Cauquoin and Werner, 2021) are the isotopic versions of ECHAM5 (Roeckner et al., 2003) and ECHAM6 (Stevens et al., 2013) models, respectively. For both ECHAM-wiso model releases, a nudged simulation was performed that covers the time period of the available isotope measurements at Concordia Station. Reanalysis data from ECMWF were used as input for nudging the iGCM: ERA-Interim Reanalysis data (Dee et al., 2011) for ECHAM5-wiso, ERA5 (Hersbach et al., 2020) for ECHAM6-wiso. ECHAM-wiso data from both nudged simulations were extracted at the nearest grid cell from Concordia Station, providing modeled daily-averaged values for the temperature at 2 m ($T_{2m\ ECHAM(5,6)}$), surface temperature ($T_{surf\ ECHAM(5,6)}$), the amount of precipitation, $\delta^{18}O$, $\delta^{2}H$, and d-excess values.

2.5 Data processing

Statistical and geostatistical analyses were performed using R 4.2.2 (R Core Team, 2022) and a number of packages, including "boot" (Canty and Ripley, 2022), "bootstrap" (Leisch, 2019), "car" (Fox and Weisberg, 2018), "caret" (Kuhn, 2022), "corrplot" (Wei and Simko, 2021), "DAAG" (Maindonald and Braun, 2011), "mgcv" (Wood, 2017), "ncdf4" (Pierce, 2023), "rcompanion" (Mangiafico, 2022), "zoo" (Zeileis and Grothendieck, 2005).

Many simple and multiple linear regression analyses were performed on the data for assessing the relationships between variables. Besides the linear models, the 95th confidence intervals (c.i.) in the prediction of the coefficients (slopes and intercept) were assessed by ordinary nonparametric bootstrap resampling (Davison and Hinkley, 1997) over at least R=2000 replicates (R larger than the input observations). The measure of performance and predictive ability of regression models were also estimated by *k*-fold cross-validation (Maindonald and Braun, 2011; James et al., 2013). This technique randomly partitions the datasets into *k* (*k*=5, in this case) equal-sized subsamples and recursively uses *k*-1 subsets of the observations to refit the regression while using the remaining part as a testing set. The root mean squared error (RMSE) and mean absolute error (MAE) were computed from residuals of original and cross-validated models as a quantitative measure of errors associated with the estimates. Trends and seasonal patterns of variables were quantified by adopting different approaches applied to the monthly-averaged data for months having at least 75% of the available records. The presence of statistically significant long-term (monotonic) linear trends during 2008-2017 was assessed through the Theil-Sen nonparametric estimator of slope (Theil, 1950; Sen, 1968) along with the Mann-Kendall test for trend (Mann, 1945; Kendall, 1975).

3. Results and Discussion

3.1 Weather and boundary layer dynamics

The time series and monthly/daily patterns of meteorological variables recorded from the AWS or modeled by ERA5 are shown in Figure S2 and S3. The full period (2008-2017) average T_{AWS} was -53°C with daily averages ranging from -82°C to -19°C and hourly values varying from -83.6°C to -14.3°C. A very high agreement between daily T_{AWS} (blue) and $T_{2m\ ERA5}$ (pink) was found (r^2=0.95). The East Antarctic Plateau is characterized by strong surface temperature inversions (Baas et al., 2019), which exhibited the same seasonal pattern of surface air temperature and ranged from -75 to -11°C. The daily inversion strength, calculated between daily radiosounding profiles and T_{AWS} varied from -6 to 48°C (Figure S2), and its temporal pattern is the mirror image of the air temperature, with higher values during the austral winters. During the coldest months (April to September), the inversion strength generally exceeds 20°C, while is less than 10°C in austral summer (Figure S3) because of the erosion due to the diurnal cycle of solar radiation.

Hourly relative humidity (RH) measured by the AWS varied from 6% to 84% (full period average 46%) with a seasonal pattern similar to air temperature. However, Genthon et al. (2013; 2017) reported frequent supersaturation events not detected by commercially available sensors. Thus, the atmospheric moisture on the Antarctic Plateau could probably be underestimated. Under this view, the relative humidity over ice (RHi) calculated from hourly ERA5 data ranged from 42 to 100% (average 64%). Figure S2 also exhibits data of RHi experimentally obtained by Genthon et al. (2017) for 2015 using hygrometry sensors modified for air sampling without artifacts. Results show hourly RHi in the 51-131% range (average 89%) with approx. 23% of 2015 over RHi 100%.

Wind roses calculated on a seasonal basis (Figure S4) show prevailing winds from the 4th quadrant (SW-S) throughout the year, peaking from the South, i.e., blowing from the highest plateau and inner regions of Antarctica. Although possible instrumental issues due to frost deposition may have led to an underestimation of wind at lower speeds, the wind blew in the 0 to 20 m s^{-1} interval (full period average: 3 m s^{-1}), with slightly higher values in November and around noon. These patterns are consistent with the literature for Dome C (e.g., Argentini et al., 2014).

Total precipitation and solar irradiation were not measured by AWS; in this study, values from ERA5 were used for total precipitation, while BSRN data were used for solar radiation. The annual cumulative amount of total precipitation during 2008-2017 ranged from approx. 20 to 30 mm y^{-1} (average 24 mm y^{-1}), in accordance with previous ERA-Interim data (1979–2012, Genthon et al., 2016). Monthly (Figure S2), precipitations were roughly

constant throughout the year with slightly lower values between October and December. The daily pattern was also quite flat, with lower values around noon. During the 2008-2017 period, the hourly average solar direct radiation was in the 0-1175 W m^{-2} range (average 345 W m^{-2}). The monthly and hourly cycles (Figure S3) clearly reflect the solar elevation patterns with the highest values recorded during the Austral summer and midday hours. SAM during 2008-2017 was predominantly positive, as reported in previous studies (Fogt and Marshall, 2020). Six main negative periods counting at least 3 continuative months with SAM index <0 were identified (May-Sept. 2009; June-Sept. 2011; Oct. 2012-Jan. 2013; Aug.-Oct. 2013; Aug.-Nov. 2014; Oct. 2016-Jan. 2017). Simple cross-correlations between the SAM index against air temperature from the AWS show only statistically significant small negative correlations at negative lags only using daily data. Results indicate that a higher daily SAM index is generally related to decreasing air temperatures after 2/3 days (all periods, DJF, MAM, JJA) and 8/9 days (SON) (Figure S5).

3.2 Water stable isotope data and its correlation with temperature

A total of 1483 daily samples were collected at Concordia Station and analyzed for the oxygen and hydrogen isotopic composition of snow. Thus, samples were collected over ~41% of days in 10 years. On a monthly basis, no precipitation was collected for 3 months (November 2009 and 2014, December 2015); approximately one third of the months include at least one week of available samples, while samples were collected on at least 90% of the days for 9 months (Figures S6 and S7). T_{AWS} during the days with collected samples was slightly (-1.6°C) but significantly (Wilcoxon rank sum test with continuity correction $p<0.05$) lower with respect to non-sampling days; at a seasonal basis, the T_{AWS} difference was -2.5°C.

Figure 1 shows the time series of the stable isotope composition data along with the air temperature measured by the AWS. $\delta^{18}O$ varied between -82.63 and -26.97‰ (average -56.7‰); $\delta^{2}H$ varied between -595.1 and -223.0‰ (average -438‰). The minimum delta values are amongst the most isotopically depleted waters collected on the Earth so far. Violin plots in Figures S8 and S9 show that data distributions were quite symmetrical (median -56.8‰ and -440‰ for $\delta^{18}O$ and $\delta^{2}H$, respectively).

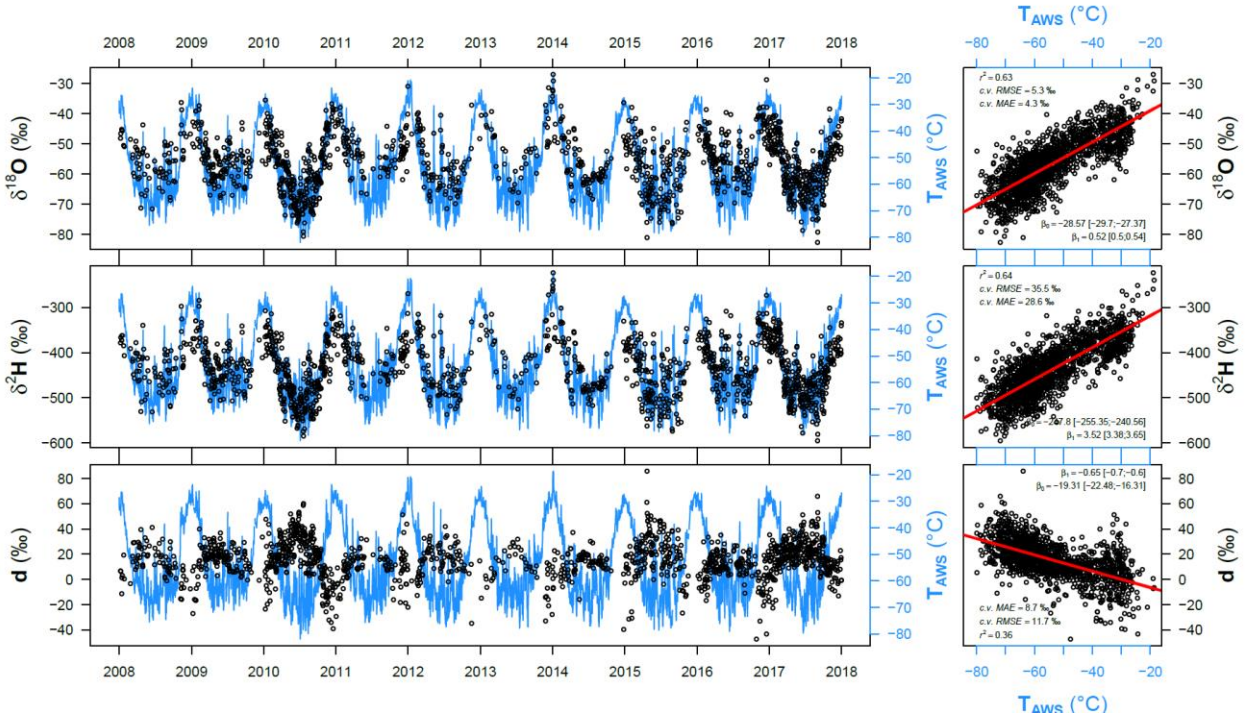

Figure 1. Left: time series of the daily averaged air temperature (blue lines) and the isotopic composition of snow (black dots) measured at Concordia during 2008-2017. Right: linear regressions between the isotopic composition of snow and air temperature.

Besides the monthly arithmetic averages, isotope data and air temperature were also computed as precipitation-weighted averages using the total precipitation amount from ERA5 (reported as $\delta^{18}O_{tp}$; $\delta^{2}H_{tp}$; d_{tp}; T_{tp}). The weighted and unweighted data and the temporal averaging time strongly depends on the lifetime of the atmospheric processes considered, a fact particularly important when dealing with precipitation in continental Antarctica, which is unevenly distributed throughout the year (Fujita and Abe, 2006; Turner et al., 2019). Indeed, the weighted $\delta^{18}O$ and $\delta^{2}H$ values are thought to be better correlated with snowfall temperature (Masson-Delmotte et al., 2008; Servettaz et al., 2023).

The monthly patterns (Figure 2) closely followed the air temperature: the lower delta values were generally recorded during the Austral winters, reflecting the "temperature effect", i.e., the positive relationship between the isotopic composition of precipitation and air temperature mainly observed at high and mid-high latitudes (Dansgaard, 1964; Rozanski et al., 1993). Generally, the lower monthly-averaged delta values were measured

335 during June ($\delta^{18}O$=-64.2‰; $\delta^{2}H$=-486‰) and the higher values in January ($\delta^{18}O$=-46.2‰; $\delta^{2}H$=-365‰). The average seasonal amplitude of delta values between DJF and JJA spanned over approx. 16‰ and 111‰ for $\delta^{18}O$ and $\delta^{2}H$, respectively.

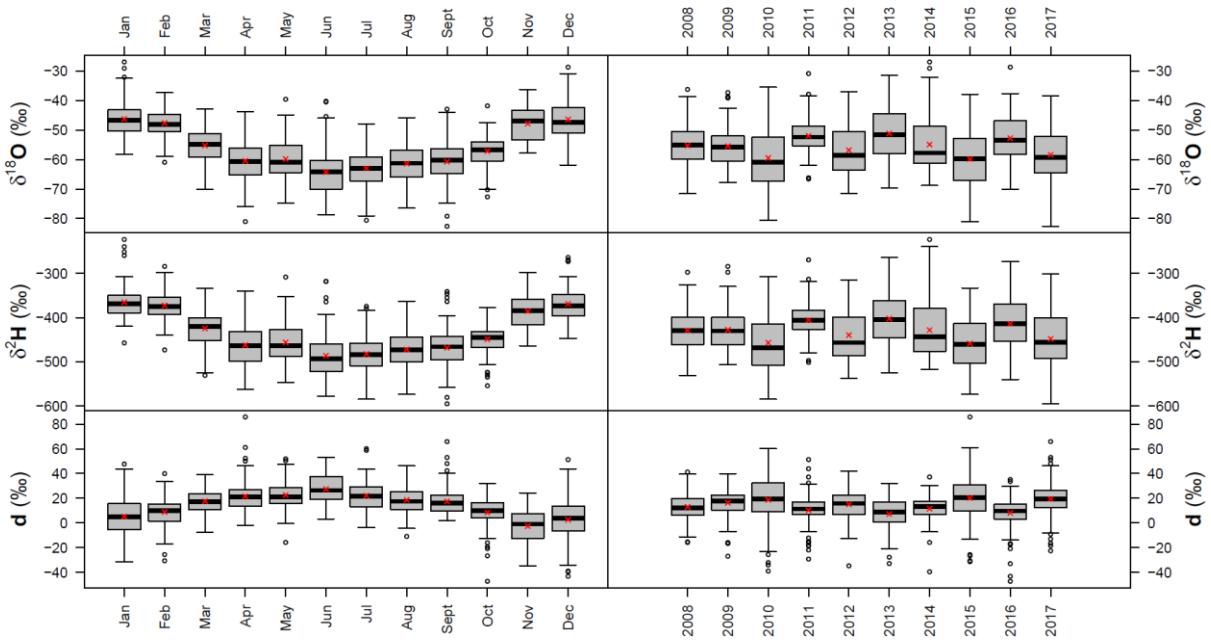

Figure 2. Seasonal (left) and annual (right) boxplots of the stable isotope composition of snow collected at Concordia
340 **station (line = median, box = inter-quartile range, whiskers=±1.5*inter-quartile range, circles = outliers and extremes; red crosses = arithmetic mean).**

The temperature effect upon the isotopic composition of precipitation is evident. Delta values exhibited a strong seasonality (Figure S10) with the less negative values recorded during Austral summers. Under this view, the
345 simple linear relationship of daily values of $\delta^{18}O$ and $\delta^{2}H$ with T_{AWS} was moderately high (r^2=0.63 and 0.64, respectively) (Figure 1; Table 1). The regression slopes were 0.52‰/°C [cross-validated 95% c.i.: 0.50-0.54‰/°C] and 3.52‰/°C [3.38-3.65‰/°C] for $\delta^{18}O$ and $\delta^{2}H$, respectively. These positive relationships become stronger on monthly-averaged data (r^2=0.82 for both $\delta^{18}O$ and $\delta^{2}H$) and slopes of 0.51 [c.i.: 0.46-0.55‰/°C] and 3.4‰/°C [c.i.: 3.09-3.73‰/°C] for $\delta^{18}O$ and $\delta^{2}H$, respectively (Figure S11; Table 1). These regressions parameters show a
350 small variability when separately computed on different years (range 0.32-0.63‰/°C). Thus, the $\delta^{18}O$-temperature

slope was almost constant during the 2008-2017, with the exception of 2011 (0.32‰/°C); when excluding 2011, the range was 0.4-0.63‰/°C. This slope range is even smaller than the confidence interval of the interannual slope [0.39; 0.83] (Table 1). On the other hand, the slope range variation over 10 years at Concordia station seems to be smaller than the spatial variation (0.6-0.91‰/°C), as reported in Masson-Delmotte et al. (2008).

Similar results were also obtained by regressing delta values against T_{AWS} weighted for tp_{ERA5}: $\delta^{18}O_{tp}$ (0.52‰/°C) and $\delta^{2}H_{tp}$ (3.56‰/°C) against T_{AWStp} (Figure S12; Table 1). Finally, regressions computed over annually-averaged data also exhibited high coefficients of determination and similar slopes (Figures S13 and S14). At annual basis, regression slopes were slightly higher: 0.59‰/°C [cross-validated 95% c.i.: 0.39-0.83‰/°C] and 3.9‰/°C [2.8-5.5‰/°C] for $\delta^{18}O$ and $\delta^{2}H$, respectively.

Table 1. Results of the regressions of delta values against air temperature.

Regression variables		Data used	Intercept		Slope		r^2	CV RMSE
Dependent	Independent		β_0 (±std. error)	BS 95th CI	β_1 (±std. error)	BS 95th CI		‰
$\delta^{18}O$	T	Daily	-29 (±1)	[-30;-27]	0.52 (±0.01)	[0.5;0.54]	0.63	5.34
$\delta^{2}H$	T	Daily	-248 (±4)	[-255;-241]	3.52 (±0.07)	[3.38;3.65]	0.64	35.5
d	T	Daily	-19 (±1)	[-22;-16]	-0.65 (±0.02)	[-0.7;-0.6]	0.36	11.7
$\delta^{18}O$	T	Monthly	-29 (±1)	[-31;-26]	0.51 (±0.02)	[0.46;0.55]	0.82	3.05
$\delta^{2}H$	T	Monthly	-251 (±8)	[-268;-232]	3.4 (±0.15)	[3.09;3.73]	0.82	20.5
d	T	Monthly	-21 (±3)	[-29;-14]	-0.65 (±0.05)	[-0.78;-0.52]	0.57	7.5
$\delta^{18}O_{tp}$	T_{tp}	Weighted monthly	-27 (±1)	[-30;-24]	0.52 (±0.02)	[0.47;0.58]	0.81	3.11
$\delta^{2}H_{tp}$	T_{tp}	Weighted monthly	-239 (±8)	[-257;-218]	3.56 (±0.17)	[3.2;3.95]	0.79	22.5
d_{tp}	T_{tp}	Weighted monthly	-21 (±3)	[-29;-15]	-0.63 (±0.05)	[-0.77;-0.52]	0.55	7.1
$\delta^{18}O$	T	Annual	-24 (±6)	[-34;-12]	0.59 (±0.12)	[0.39;0.83]	0.75	1.6
$\delta^{2}H$	T	Annual	-223 (±41)	[-280;-140]	3.9 (±0.77)	[2.78;5.5]	0.76	10.3
d	T	Annual	-30 (±13)	[-56;-4]	-0.82 (±0.23)	[-1.3;-0.33]	0.61	3.2
$\delta^{18}O_{tp}$	T_{tp}	Weighted annual	-22 (±6)	[-40;-9]	0.62 (±0.14)	[0.24;0.93]	0.71	1.7
$\delta^{2}H_{tp}$	T_{tp}	Weighted annual	-188 (±50)	[-338;-81]	4.52 (±1.08)	[1.25;6.88]	0.69	13.9
d_{tp}	T_{tp}	Weighted annual	-13 (±10)	[-30;6]	-0.48 (±0.22)	[-0.84;-0.06]	0.37	2.4

3.3 Local meteoric water lines

The local meteoric water line (LMWL) reveals the linear relationship between $\delta^{18}O$ and $\delta^{2}H$ (Craig, 1961; Dansgaard, 1964). LMWLs were computed by considering all single samples from the entire study period (Figure 3) as well as using aggregated data for the entire dataset or over each season. Regression statistics are also summarized in Table 2; the regression coefficients were always statistically significant (p<0.05). The LMWL computed over daily data was (r^2=0.98):

$$\delta^{2}H = 6.65\ [6.59;6.71] \cdot \delta^{18}O - 60.72\ [-64.3;-57.1]$$

with a prediction error for $\delta^{2}H$ of 8.4‰ (5-folds cross-validated RMSE); these results are very similar to the values for the 2008-2010 period ($\delta^{2}H = 6.5 \cdot \delta^{18}O - 68.8$) reported by Stenni et al. (2016). The LMWL computed over monthly-averaged data weighted for ERA5 total precipitation was:

$$\delta^{2}H_{tp} = 6.83\ [6.64;7.07] \cdot \delta^{18}O_{tp} - 52.29\ [-62.43;-37.81]$$

The intercepts (β_0) and slopes (β_1) of all LMWLs computed with different data and periods are summarized in Figure 4 along with their cross-validated c.i. Generally, the coefficients of the regressions for the weighted and unweighted monthly data return very similar results over the 4 seasons when accounting for the confidence intervals (Table 2). On the contrary, the LMWLs calculated at a seasonal basis (Figure 4, color symbols) generally show lower slopes (6.02 [c.i.: 5.73;6.32]) and intercepts (-86.76 [c.i.: -101;-72]) in Austral summers, while higher regression coefficients were recorded in autumns (slope 6.72 [6.58;6.82], intercept -54 [-63;-49]), clearly depicting the seasonal effect over the isotopic composition. Monthly LMWLs on weighted data show slightly higher intercepts and slope values than the daily and unweighted monthly data (Table 2). In all cases, summer LMWLs show lower r^2 compared to the other seasons as well as to the entire dataset.

The slope of the LMWL exhibits lower values than the 7.75 obtained by Masson-Delmotte et al. (2008) for the whole Antarctic surface snow database, although in better agreement with the one obtained for the last quartile of the isotopic distribution and corresponding to 7.28, for isotopic $\delta^{18}O$ values of surface snow below -42.8‰. This reflects the lower slope of the MWL when dealing with very depleted precipitation at the final stages of the isotopic distillation line. In agreement with theoretical isotopic models (Jouzel and Merlivat, 1984), the MWL slopes in surface snow of East Antarctica decrease from the coastal areas to the inland plateau (Masson-Delmotte et al., 2008). This decrease directly impacts on the d-excess values (see next section). However, when considering

395 the MWL calculated on the annual average data weighted for ERA5 total precipitation, the slope (7.33) is in very good agreement with the one reported from Masson-Delmotte et al. (2008). Indeed, the surface snow data consider the first few meters of the snowpack, which corresponds, in theory, to the precipitation of several years already "naturally" weighted for precipitation.

400

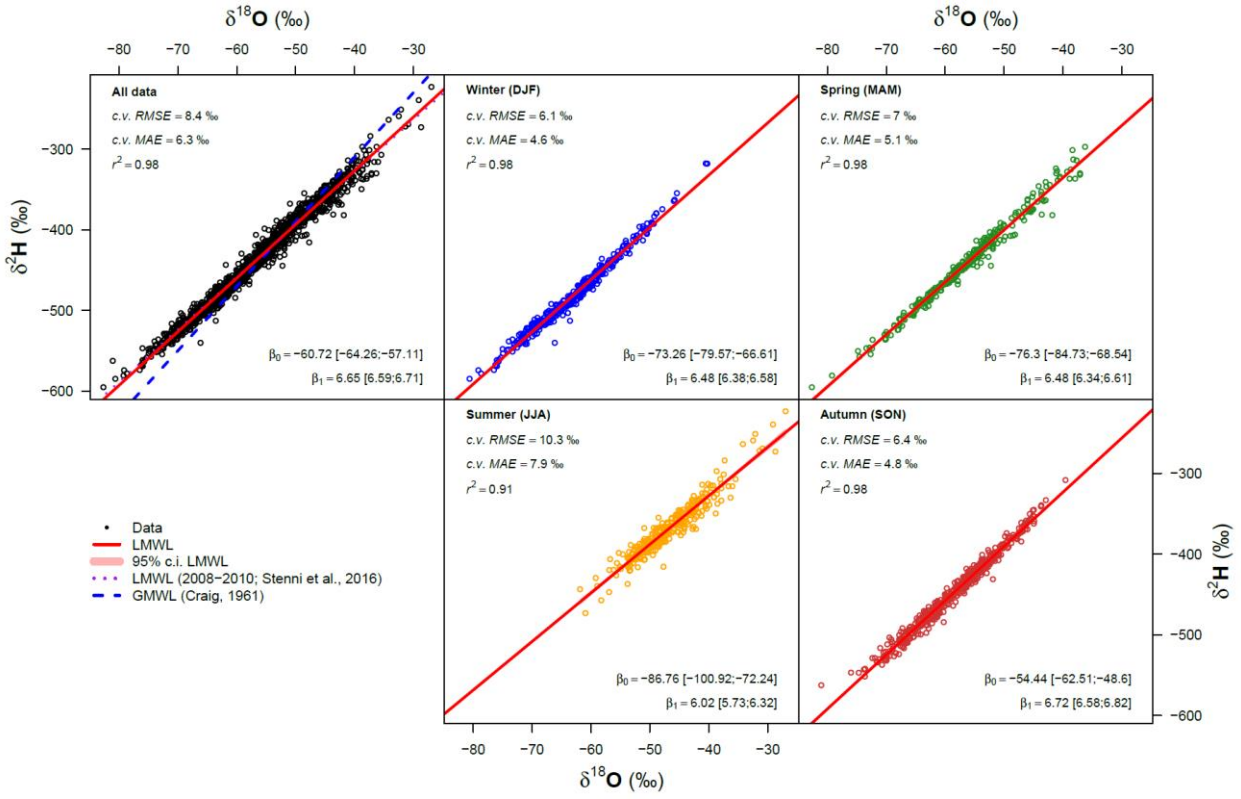

Figure 3. Local meteoric water lines computed on the isotopic composition of the daily samples for the entire dataset (upper left) and for the single seasons. Regression parameters are also summarized in Table 2. The plot for all data also illustrates LMWLs reported by Stenni et al. (2016) and the global meteoric water line by Craig (1961).

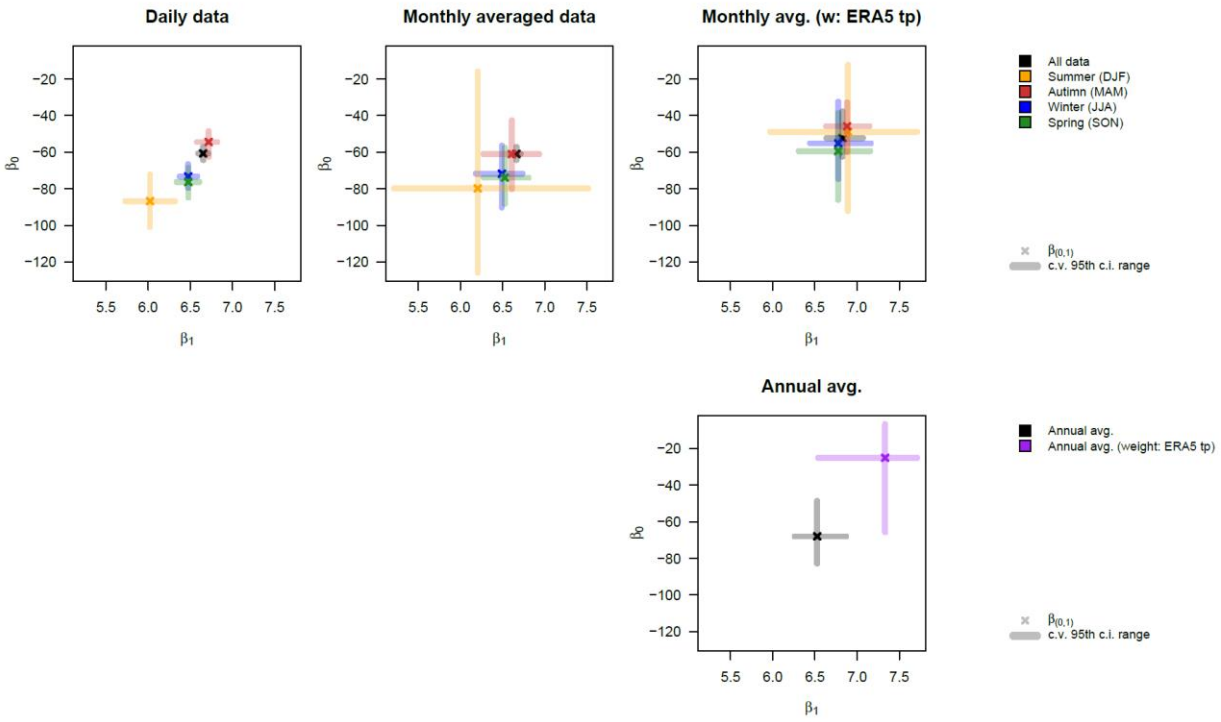

405

Figure 4. Intercepts (β_0) and slopes (β_1) of all computed LMWLs along with their cross-validated confidence intervals.

410

415

Table 2. Local meteoric water lines (LMWLs) computed over different time periods.

Regr. Variables		Data used	Intercept		Slope		r^2	CV RMSE
DV	IV		β_0 (±std. error)	BS 95th CI	β_1 (±std. error)	BS 95th CI		‰
δ^2H	$\delta^{18}O$	Daily, all data	-61 (±1)	[-64;-57]	6.65 (±0.02)	[6.59;6.71]	0.98	8.4
δ^2H	$\delta^{18}O$	Daily, W (JJA)	-73 (±3)	[-80;-67]	6.48 (±0.05)	[6.38;6.58]	0.98	6.1
δ^2H	$\delta^{18}O$	Daily, SP (SON)	-76 (±3)	[-85;-69]	6.48 (±0.05)	[6.34;6.61]	0.98	7
δ^2H	$\delta^{18}O$	Daily, SU (DJF)	-87 (±5)	[-101;-72]	6.02 (±0.11)	[5.73;6.32]	0.91	10.3
δ^2H	$\delta^{18}O$	Daily, F (MAM)	-54 (±3)	[-63;-49]	6.72 (±0.04)	[6.58;6.82]	0.98	6.4
δ^2H	$\delta^{18}O$	Monthly, all data	-61 (±4)	[-69;-49]	6.66 (±0.07)	[6.53;6.87]	0.99	5.9
δ^2H	$\delta^{18}O$	Monthly, W (JJA)	-72 (±9)	[-90;-56]	6.49 (±0.14)	[6.18;6.74]	0.99	3.6
δ^2H	$\delta^{18}O$	Monthly, SP (SON)	-74 (±7)	[-88;-58]	6.53 (±0.12)	[6.28;6.81]	0.99	4.4
δ^2H	$\delta^{18}O$	Monthly, SU (DJF)	-80 (±21)	[-126;-16]	6.21 (±0.44)	[5.21;7.52]	0.88	7.2
δ^2H	$\delta^{18}O$	Monthly, F (MAM)	-61 (±9)	[-80;-43]	6.61 (±0.15)	[6.27;6.93]	0.99	3.4
δ^2H_{tp}	$\delta^{18}O_{tp}$	Weighted monthly, all data	-52 (±4)	[-62;-38]	6.83 (±0.08)	[6.64;7.07]	0.98	6.3
δ^2H_{tp}	$\delta^{18}O_{tp}$	Weighted monthly, W (JJA)	-55 (±8)	[-75;-32]	6.78 (±0.14)	[6.44;7.16]	0.99	3.9
δ^2H_{tp}	$\delta^{18}O_{tp}$	Weighted monthly, SP (SON)	-59 (±8)	[-86;-39]	6.78 (±0.15)	[6.31;7.16]	0.99	5.4
δ^2H_{tp}	$\delta^{18}O_{tp}$	Weighted monthly, SU (DJF)	-49 (±18)	[-92;-12]	6.89 (±0.41)	[5.97;7.71]	0.91	9.3
δ^2H_{tp}	$\delta^{18}O_{tp}$	Weighted monthly, F (MAM)	-46 (±7)	[-60;-33]	6.88 (±0.14)	[6.63;7.15]	0.99	3.1
δ^2H	$\delta^{18}O$	Annual	-68 (±9)	[-83;-49]	6.53 (±0.17)	[6.26;6.87]	0.99	1.5
δ^2H_{tp}	$\delta^{18}O_{tp}$	Weighted annual	-25 (±15)	[-66;-7]	7.33 (±0.29)	[6.54;7.71]	0.99	2.3

3.4 Deuterium excess

Deuterium excess varied between -47.3 and 85.8‰ (average 15.6‰); the violin plots for the whole period (Figure S8-9) show quite symmetrical data distributions (median 15.7‰). The seasonal pattern (Figure 2) inversely followed the air temperature, with higher d-excess is generally recorded during Austral winters (average JJA 22.5‰, average DJF 5.9‰). The average seasonal amplitude of d-excess variations between DJF and JJA was 17‰. The linear relationships between d-excess and T_{AWS} were weaker than for $\delta^{18}O$ and δ^2H (r^2=0.36 to 0.61; Table 1), with regression slopes of -0.65‰/°C for daily data. This relationship is slightly stronger using monthly averaged data (r^2=0.57) with a slope of -0.65‰/°C and -0.63‰/°C for the monthly averaged and the monthly weighted averages, respectively. Annually-averaged data show a higher slope (-0.82‰/°C) and an even stronger relationship (r^2=0.61) when using unweighted values.

Deuterium excess exhibits a statistically significant (p<0.05) negative linear relationship with $\delta^{18}O$ on daily data (r^2=0.67), showing a slope of -1.35 (Figure S16; Table S1), slightly higher than the value of -1.5 reported by Stenni et al. (2016) for 2008-2010. The linear relationship on daily data is even higher in winter and spring (r^2=0.75), but lower in summer (r^2=0.53) (Figure S16). Using the monthly unweighted and weighted data, the slopes are respectively -1.34 and -1.18 for the whole dataset. These relationships are summarized in Figure 5.

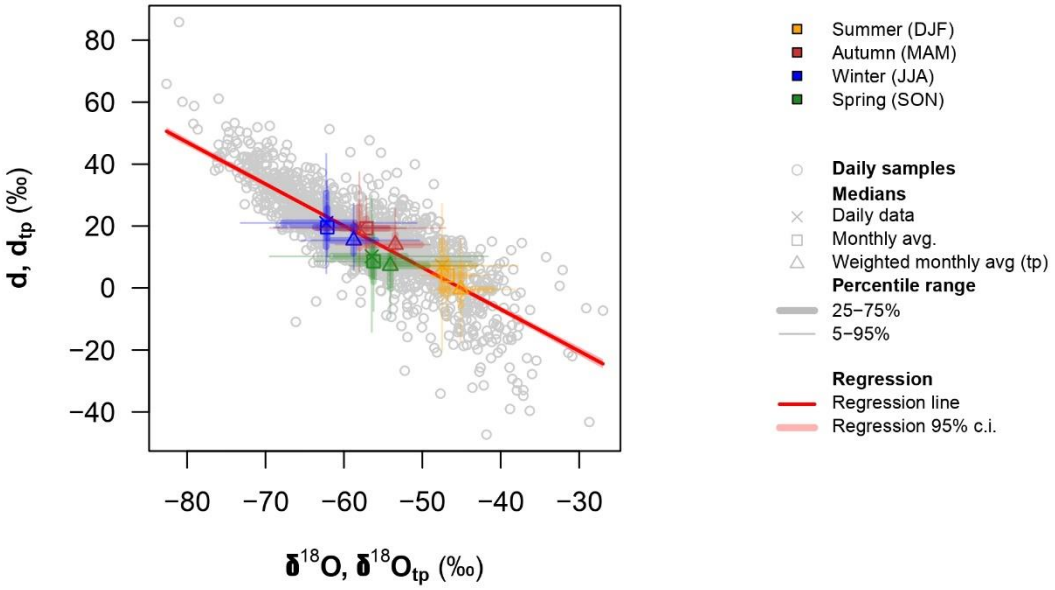

Figure 5. Relationships between $\delta^{18}O$ and d-excess. The red line represents the linear fit of the data.

The linear relationship between $\delta^{18}O$ and d-excess computed on the annual-averaged data returns a high coefficient of determination (R^2=0.91), however, the one computed on weighted data exhibits a much worse fit.

An anticorrelation between delta values and d-excess has been already reported in precipitation at Dome C (Stenni et al., 2016) and across continental Antarctica, e.g., at Vostok (Ekaykin et al., 2004) and Dome F (Fujita and Abe, 2006), while it was not observed for coastal areas, e.g., Dronning Maud Land (Schlosser et al., 2008) and Law Dome (Delmotte et al., 2000).

The high d-excess values encountered in winter precipitation and the large seasonal amplitude cannot be only explained by a change in the moisture source regions, but its increase might be related to the very low condensation temperature and its effect on d-excess, as well as to the decrease in the slope of the MWL at very low temperatures (Touzeau et al., 2016). Indeed, as previously reported in Craig (1961) and Uemura et al. (2012), any process which

deviates from the average δ^2H-$\delta^{18}O$ slope 8 (GMWL) can affect the d-excess parameter. To this end, we calculated the logarithmic version of d-excess to assess whether the observed δ^2H-$\delta^{18}O$ of precipitation better fit a curve rather than a straight line (Uemura et al., 2012), as in the canonical definition of d-excess following the GMWL. The logarithmic transformation effectively reduces the sensitivity of the observed d-excess to observed $\delta^{18}O$ (slope from -1.35 to -0.58) and almost flattened the sensitivity of the observed d-excess to observed δ^2H (slope from -0.18 to -0.03). Such a smaller sensitivity between δ values and d-excess for the logarithmic transformation highlights that special attention should be paid when dealing with extremely depleted precipitation, since the linear approximation introduced by the GMWL does not hold anymore. This is especially true when attempting to extrapolate any relationship between precipitation d-excess in extremely cold regions and the evaporative conditions of warmer moisture sources. Moreover, different processes might be involved on the precipitation sample before the collection, such as mixing with wind-drifted snow and sublimation (Ritter et al., 2016), which could translate into a smaller $\delta^{18}O$ vs δ^2H slope for precipitation samples. The d-excess/$\delta^{18}O$ ratios were analyzed to better trace the effects of possible sublimation processes (Figure S17). Seasonally, the ratios closely follow the pattern of air temperature. While most of the ratio values generally led between 0 and -0.7, positive values are also found during Austral summer and spring. Positive ratios depict negative values of d-excess; extremely positive values, 0.5 up to 1.5, are recorded in the Austral summer.

The d-excess/$\delta^{18}O$ relationship was stronger during winter and spring and weaker in summer (Table S1), possibly reflecting the effects of sublimation, due to 24-hour summer solar irradiance, during the permanence of snow on the benches before sampling. Sublimation effects, acting preferentially during summer, explain the negative values of d-excess mostly found in the summer period (Casado et al., 2021).

3.5 Correlations between water stable isotope data and meteorological parameters

The daily and monthly-averaged isotope data were analyzed to detect the pairwise correlations with other measured or modeled variables. Since the data distribution of some variables is not normal, the nonparametric Kendall's rank correlation τ was computed. Delta values were significantly (p<0.05) and moderately (0.35<τ<0.6) to highly (τ>0.6) correlated with air temperature, the temperature of the inversion layer (T_{INV}), RH, surface pressure and direct solar radiation, both using daily (Figure S18) and monthly-averaged (Figure S19) data. On the contrary, d-excess was anticorrelated with the temperature of the inversion layer (T_{INV}), and RH. Correlations between weather variables reveal positive relationships between air temperature, T_{INV}, RH, surface pressure and direct solar radiation. These relationships were generally observed during the whole 2008-2017 period and singularly during the Austral autumn, winter, and spring, while correlations in summer (DJF) were generally

lower. This latter result might depict the effects of the maximum insolation and possible post-depositional processes upon the isotopic composition of precipitation. Under this view, large diurnal cycles in both surface air temperature and humidity in summer may result from either boundary layer dynamics and/or air–snow sublimation/condensation exchanges (Casado et al., 2016). Generally, SAM was not correlated with any other variable except surface pressure.

No statistically significant (p<0.05) long-term linear trends were identified by the Mann-Kendall test for trends during 2008-2017, either using all the monthly-averaged data or analyzing each season separately.

4. Comparisons with ECHAM5-wiso and ECHAM6-wiso simulations

The outputs of the ECHAM5-wiso and ECHAM6-wiso model releases are compared with experimental data. In this paper, we mainly focused on ECHAM6-wiso model results while in the SI we also reported the comparison between observations (collected precipitation) and ECHAM5-wiso.

For these comparisons there are some limitations to consider. First, until 2010 samples were collected when at least 5 mL of water equivalent of snow was found on the platform to allow for analysis using the IRMS-equilibration technique, while smaller samples were collected later due to the availability of the CRDS technique in the laboratory, which requires a smaller amount of water. Thus, the initial experimental data could be representative of higher accumulation events on the bench which could be caused by more intense precipitation events as well as by a significant amount of wind-drifted snow. The samples collected on the platform could also be affected by snow blown either in or out by winds. Finally, although the operators monitored the platform on a daily basis, post-depositional modification of the isotopic composition of the samples may have happened due to sublimation and/or condensation.

ECHAM5-wiso model simulated 2900 precipitation events in 2008-2017, while ECHAM6-wiso reports 3017, i.e., both models simulated about twice as many precipitation days compared to the experimentally collected samples. Four cases can be observed with respect to the agreement or disagreement between the models and the experimental observations, as reported in Figures S20 and S21 (both no precipitation, both precipitation, precipitation only on experimental samples, and precipitation only simulated by models). Figures show that both model versions (ECHAM5-wiso and ECHAM6-wiso) simulated no precipitation when no sample was collected in the platform for about 13% of the days. Conversely, model results imply that precipitation and snow samples were collected during 37% of the period. This result indicates that for half of the period under consideration there

was agreement/disagreement between models and collected snow. In particular, the greatest difference (46% of the period) is found when the models simulate precipitation while no sample was collected at Concordia.

The reason for this difference is not clear. Figures S20 and S21 also report the amount of precipitation estimated by ERA5 in the 4 cases, i.e., when the models and experimental observations agree or not. Precipitation rates from ERA5 are very small for days when both ECHAM-wiso model versions and experimental observations report no precipitation, while significantly higher values are modeled when both have snow. However, for days when there is a disagreement between models and collected samples, ERA5 predicts less precipitation when only samples have been collected. This could indicate samples affected by snowdrift; however, there are no major differences in wind speed between the 4 groups to support this hypothesis. Evaporation estimated by ERA5 also shows no strong variation between the 4 cases. Instead, there are significant differences for air temperature, RH, and direct solar irradiance, all weather variables showing strong seasonality (Figure S3).

Figure 6 shows the time series of the delta values analyzed experimentally and modeled by the ECHAM6-wiso model (the comparison between delta values from ECHAM5-wiso and experimental data is shown in figure SI22). Modeled $\delta^{18}O$ varied between -105 and -25‰ (average -53.8‰) while modeled $\delta^{2}H$ varied between -938 and -191‰ (average -424‰) in ECHAM6-wiso. Modeled d-excess spans between -97‰ and 86‰ (average 7‰) with a standard deviation of 10‰, which is 5‰ smaller than the one observed for precipitation. The violin plots in Figures S8 and S9 show that data distributions were quite wider than the experimental data, especially in the case of ECHAM5-wiso. Overall, the $\delta^{18}O$ and $\delta^{2}H$ simulated data were less negative than the observations with a larger difference during winter and summer.

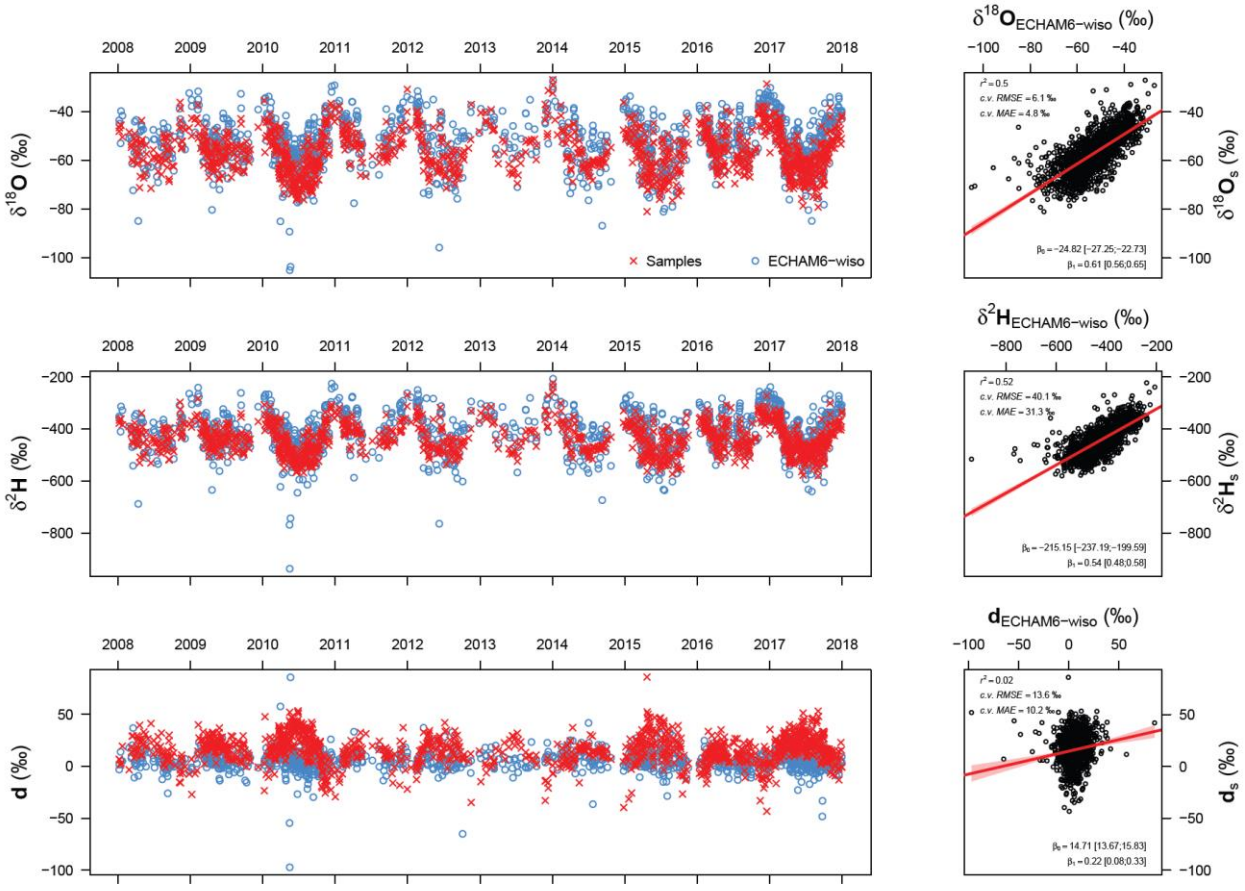

530

Figure 6. Time series of the delta values analyzed experimentally (red crosses) and modeled by the ECHAM6-wiso model (blue circles) and their linear regressions. The scatter plots report only the days with both experimental and modeled precipitation data.

535 The linear relationships between observations and simulated daily data from ECHAM6-wiso are reported in Figure 6. Moderately good relationships were found for $\delta^{18}O$ (r^2=0.5) and δ^2H (r^2=0.52) values, while no relationship was found for d-excess (r^2=0.02) (Figures S24 and S25).

Figure 7 reports the comparison of the seasonal variations of experimentally determined data (observations) and simulated data from ECHAM6-wiso, which confirms the overestimation (less negative values) of the model $\delta^{18}O$

540 and δ^2H data compared to observations. Larger overestimations are found in summer for both isotopic ratios,

particularly in December and January. For $\delta^{18}O$ alone, a larger overestimation is also found in June (winter). This overestimation was also present in the simulated T_{2m} compared to T_{AWS}, which could in part explain the overestimated isotopic values, although no significant correlation exists between the difference of observed and modeled temperatures vs the observed and modeled isotopic values.

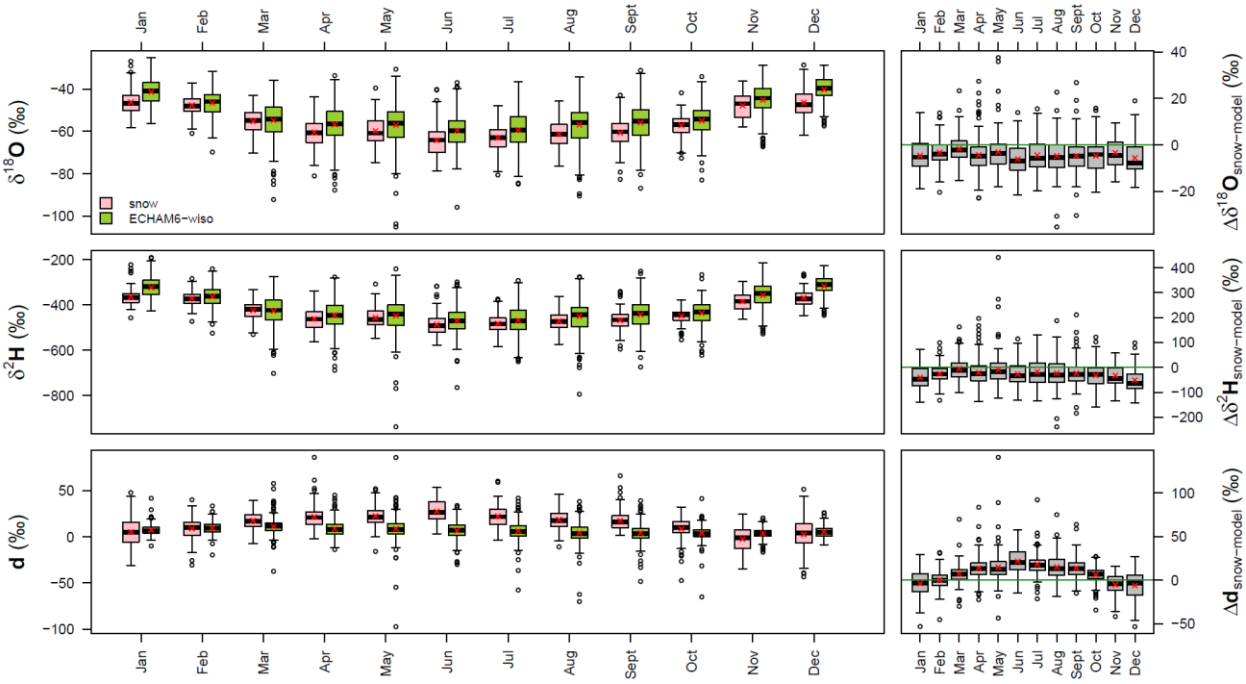

545

Figure 7. Seasonal variation of the experimentally measured isotopic data and ECHAM6-wiso modeled data (left) and their differences (right); line = median, box = inter-quartile range, whiskers = ±1.5*inter-quartile range, circles = outliers and extremes; red crosses = arithmetic mean.

A moderate linear relationship is found between the observed and modeled d-excess vs temperature (r^2=0.27), which might indicate the effect of seasonality in model performances simulating kinetic fractionation or non-resolved sub-grid processes. Indeed, such relationship is more scattered during summer and winter ($r^2 \leq 0.06$) and more robust during spring (r^2=0.30).

The local meteoric water lines (LMWLs) computed over different time periods using ECHAM6-wiso outputs are reported in Table S5. The slope (β_1) obtained from all daily data is 7.66 (±0.02), in good agreement with the one obtained from Masson-Delmotte et al. (2008) for the whole Antarctic surface snow data set (7.75), but slightly higher than the one for the more negative inland values (7.28). On the contrary, ECHAM5-wiso simulated lower slope values (Table S3; 6.22±0.03), in better agreement with observations from this study (6.65 ±0.02).

The simulated d-excess showed the largest discrepancies. Overall, a smaller seasonal amplitude was observed in the d-excess simulated data with the largest discrepancy in winter, which showed lower values than observations; however, the tuning of the supersaturation function could contribute to the d-excess discrepancy.

The relationship between isotopic ratios and temperature simulated by ECHAM6-wiso (Figure S23 and Table S4) exhibited slightly higher slopes than the observed data. The simple linear relationship of daily values of $\delta^{18}O$ and $\delta^{2}H$ with T_{2m} was moderate (r^2=0.5 and 0.53, respectively). The regression slopes were 0.67‰/°C [cross-validated 95% c.i.: 0.65-0.69‰/°C] and 5.34‰/°C [5.17-5.51‰/°C] for $\delta^{18}O$ and $\delta^{2}H$, respectively. These positive relationships become stronger on monthly-averaged data (r^2=0.88 and 0.9 for $\delta^{18}O$ and $\delta^{2}H$, respectively) with slopes values of 0.61‰/°C [c.i.: 0.57-0.65‰/°C] and 4.87‰/°C [c.i.: 4.6-5.17‰/°C] for $\delta^{18}O$ and $\delta^{2}H$, respectively. Finally, regressions computed over annually-averaged unweighted simulated data exhibited high coefficients of determination but higher slopes (Table S4). At annual basis, regression slopes were 0.87‰/°C [cross-validated 95% c.i.: 0.43-1.13‰/°C] and 7.36‰/°C [4.22-9.36‰/°C] for $\delta^{18}O$ and $\delta^{2}H$, respectively. Interestingly, if looking at precipitation-weighted annual data these slopes became very low (0.28 and 2.6), but with low coefficients of determination (0.29 and 0.34), for both $\delta^{18}O$ and $\delta^{2}H$, respectively.

The results of the comparison between observations and simulated data using the outputs from ECHAM6-wiso are in relatively good agreement with what previously reported by Goursaud et al. (2018) in their comparison using model outputs from ECHAM5-wiso and field data from the whole Antarctic continent. They also found a warm model bias over central Antarctica as observed in the present study and an overall agreement in the spatial distribution of the isotopic values.

5. Conclusions

In this study, we presented a 10-year record of the isotopic composition ($\delta^{18}O$, $\delta^{2}H$ and d-excess) of daily-collected precipitation samples at Concordia Station, East Antarctica, from 2008 to 2017; this represents a unique dataset for inland Antarctica. Despite the difficulties related to collecting samples in such a harsh environment, especially during the Antarctic winter, the daily work of the winter-over personnel of Concordia Station has allowed to build an unprecedented database which will be of extreme importance for interpreting the climate record from oxygen and hydrogen stable isotopes that the Beyond EPICA 1.5 million year ice core will soon provide, as well as other East Antarctic ice core isotopic records. To this end, a

comprehensive statistical analysis was performed on our precipitation isotopic data, correlated with the instrumental meteorological records and the outputs from the isotope-enabled ECHAM5-wiso and ECHAM6-wiso model versions.

The bench used to collect precipitation stands one meter from the ground and is shielded by an 8-cm rail on three out of four sides, but wind scouring might still remove part of the accumulation and wind-drifted snow might still contribute to the deposition collected on the bench, altering the original isotopic composition of precipitation. During summer months, the snow on the bench might also be subjected to sublimation due to the direct solar irradiation for the hours preceding the sampling; this could explain the occurrence of negative d-excess values in this season. Despite these limitations, the dataset presented in this study is the closest we could get to daily precipitation for a continuous 10-year period at Concordia.

The precipitation isotopic composition and the surface temperature showed a marked seasonal variation over the investigated period with a moderately high linear relationship at the daily scale. The relationship becomes stronger when using monthly averages. The $\delta^{18}O$ (and $\delta^{2}H$) to T_{AWS} slope of 0.52‰/°C (and 3.52‰/°C) computed on the daily values slightly increases to 0.59‰/°C (and 3.9‰/°C) when computed over annually averaged data, although no statistically significant ($p<0.05$) long-term linear trends were identified during the 2008-2017 period.The LMWL computed over the entire dataset, as well as those calculated for each season, are characterized by lower slopes compared to the 7.75 value found by Masson-Delmotte et al. (2008) for Antarctic surface snow, and also lower than the 7.28 reported in the same study for $\delta^{18}O$ values below -42.8‰. Even lower slopes are observed in this study when considering only summer (DJF) data, with a slightly worse determination coefficient; this seasonal bias might also be due to the effect of sublimation (Ritter et al., 2016; Casado et al., 2021). The high d-excess values found in winter, as well as its seasonal amplitude, are mostly due to the extremely low condensation temperature rather than to changes in moisture origin. The 10-year dataset of the isotopic composition of precipitation presented in this study has allowed us to perform a comparison between the observed and modeled (ECHAM5 and ECHAM6-wiso) $\delta^{18}O$ and $\delta^{2}H$ of precipitation. ECHAM6-wiso showed, on average, less negative simulated delta values compared to the measured samples, with larger differences during winter, spring and summer and smaller differences observed in autumn. The different d-excess output from the two model versions could be caused by minor changes in the equation of the supersaturation function, as well as by differences in the modeled influence of the sea ice and the different treatment of wind speed influence on kinetic fractionation during evaporation processes. It is also worth mentioning that ECHAM5-wiso is nudged to ERA-interim while ECHAM6-wiso is nudged to ERA5.

ECHAM6-wiso also better captured the amplitude of seasonal variations compared to ECHAM5-wiso. The LMWL computed over ECHAM5-wiso daily data returned a slope of 6.22, while ECHAM6-wiso daily data provided a slope of 7.66, which is similar to the one found by Masson-Delmotte et al. (2008) for Antarctic surface snow (7.75), but higher than the one obtained with measured data (6.65) in this study. However, we have to consider that while ECHAM-wiso models simulate the isotopic composition of precipitation, the snow we sample on the bench is the result of precipitation combined with possible post-depositional processes such as sublimation and snow blown onto or off the platform by the wind.

To conclude, the dataset presented here represents a unique record, which, together with the meteorological data, will provide a valuable contribution for the comprehension of the mechanisms determining the isotopic composition of precipitation in

inland Antarctica and will hopefully benefit the ice core record climatic interpretation in the future. The isotopic composition of precipitation dataset could also be used as the input of isotope-enabled snowpack models.

The collection of daily precipitation samples at Dome C is still ongoing and the data since 2018 will be presented in future publications within the ITN DEEPICE project, where the 2017-2021 dataset will also be compared to surface and sub-surface snow samples at Concordia.

Data availability

Isotope data are made available in Zenodo: https://doi.org/10.5281/zenodo.10197160. ERA5 hourly data on single levels from 1940 to present are available through the Copernicus Climate Data Store (CDS) at: https://doi.org/10.24381/cds.adbb2d47 (Hersbach et al., 2023). The Antarctic Meteo-Climatological Observatory AWS Concordia data are available upon request at https://www.climantartide.it/dataaccess/AWS_CONCORDIA/index.php?lang=en (Grigioni et al., 2022a). Dome C II AMRC AWS are available at ftp://amrc.ssec.wisc.edu/pub/aws/q1h/. Radiosounding data are available upon request at https://www.climantartide.it/dataaccess/RDS_CONCORDIA/index.php?lang=it (Grigioni et al., 2022b). The Baseline Surface Radiation Network (BSRN) data are available at https://bsrn.awi.de/data/data-retrieval-via-pangaea/. AAO (SAM) index monthly data are available at https://www.cpc.ncep.noaa.gov/products/precip/CWlink/daily_ao_index/aao. The CALVA project and CENECLAM and GLACIOCLIM observatories data are available at https://web.lmd.jussieu.fr/~cgenthon/SiteCALVA/CalvaData.html. The ECHAM5-wiso and ECHAM6-wiso used in this study are published in the Zenodo database (https://doi.org/10.5281/zenodo.11468043, Cauquoin and Werner, 2024). The full dataset used for the present publication is also available in Zenodo (https://doi.org/10.5281/zenodo.11613330) and includes daily data, monthly averaged data, precipitation weighted monthly averages, annual averaged data, and precipitation weighted annual averaged data.

Author contributions

GD and BS designed the research. GD, BS and VP performed the lab analysis. MW and AC provided the ECHAM-wiso data. MM performed the data analysis. MM, GD and BS drafted the first version of the paper. DZ, CS, VC, MC, AL, MW, AC, GC and MDG contributed to the writing of the paper. GC provided valuable information on precipitation sampling.

Competing interests

The contact author has declared that none of the authors has any competing interests.

Acknowledgements

Meteorological dataset and information are achieved by the Italian Antarctic Meteo-Climatological Observatory (IAMCO) https://www.climantartide.it in the framework of the PNRA/IPEV 'Routine Meteorological Observation at Station Concordia' project. We acknowledge using data from: (i) the CALVA project and CENECLAM and GLACIOCLIM observatories; (ii) the Baseline Surface Radiation Network (BSRN, https://bsrn.awi.de/). We also acknowledge Quantarctica and the Norwegian Polar Institute for providing the ETOPO1, IBCSO, and RAMP2 data for basemap usage, the U.S. National Ice Center (USNIC) for providing a shapefile with polygons representing Antarctic ice shelfs and land features, the UK Polar Data Centre, Natural Environment Research Council, UK Research & Innovation for providing the medium resolution vector polygons of the Antarctic coastline. The precipitation measurements at Dome C as well as the isotopic analysis have been conducted in the framework the projects PNRA 2013/AC3.05 (PRE-REC) and PNRA18_00031 (WHETSTONE) of the Italian National Antarctic Research Program "Programma Nazionale di Ricerche in Antartide" (PNRA) funded by MIUR (now MUR). We would also like to thank the logistics staff and winter-over crews at Concordia station for all the investigated periods.

References

Argentini, S., Pietroni, I., Mastrantonio, G., Viola, A. P., Dargaud, G., and Petenko, I.: Observations of near surface wind speed, temperature and radiative budget at Dome C, Antarctic Plateau during 2005, Antarct. Sci., 26, 104–112. https://doi.org/10.1017/S0954102013000382, 2014.

Baas, P., van de Wiel, B. J. H., van Meijgaard, E., Vignon, E., Genthon, C., van der Linden, S.J.A., and de Roode, S. R.: Transitions in the wintertime near-surface temperature inversion at Dome C, Antarctica, Q. J. R. Meteorol. Soc., 145, 930–946, https://doi.org/10.1002/qj.3450, 2019.

Bai, J., Zong, X., Lanconelli, C., Lupi, A., Driemel, A., Vitale, V., Li, K., and Song, T.: Long-Term Variations of Global Solar Radiation and Its Potential Effects at Dome C (Antarctica), Int. J. Environ. Res. Public Health, 19(5), 3084, https://doi.org/10.3390/ijerph19053084, 2022.

Bromwich, D. H., Guo, Z. C., Bai, L. S., and Chen, Q. S.: Modeled Antarctic precipitation. Part I: Spatial and temporal variability, J. Clim., 17, 427–447, https://doi.org/10.1175/1520-0442(2004)017%3C0427:MAPPIS%3E2.0.CO;2, 2004.

Buizert, C., Fudge, T. J., Roberts, W. H. G., Steig, E. J., Sherriff-Tadano, S., Ritz, C., Lefebvre, E., Edwards, J., Kawamura, K., Oyabu, I., Motoyama, H., Kahle, E. C., Jones, T. R., Abe-Ouchi, A., Obase, T., Martin, C., Corr, H., Severinghaus, J. P., Beaudette, R., Epifanio, J. A., Brook, E. J., Martin, K., Chappellaz, J., Aoki, S., Nakazawa, T., Sowers, T. A., Alley, R. B., Ahn, J., Sigl, M., Severi, M., Dunbar, N. W., Svensson, A., Fegyveresi, J. M., He, C., Liu, Z., Zhu, J., Otto-Bliesner, B. L., Lipenkov, V. Y., Kageyama, M., and Schwander, J.: Antarctic surface temperature and elevation during the Last Glacial Maximum, Science (80), 372, 1097–1101, https://doi.org/10.1126/science.abd2897, 2021.

Davison, A.C. and Hinkley, D. V.: Bootstrap Methods and Their Application, Biometrics, https://doi.org/10.2307/3109789, 1998.

Canty, A. and Ripley, B. boot: Bootstrap R (S-Plus) Functions. R package version 1.3-28.1, https://CRAN.R-project.org/package=boot, 2022.

Casado, M., Landais, A., Masson-Delmotte, V., Genthon, C., Kerstel, E., Kassi, S., Arnaud, L., Picard, G., Prie, F., Cattani, O., Steen-Larsen, H. C., Vignon, E., and Cermak, P.: Continuous measurements of isotopic composition of water vapour on the East Antarctic Plateau, Atmos. Chem. Phys., 16, 8521–8538, https://doi.org/10.5194/acp-16-8521-2016, 2016.

Casado, M., Orsi, A., and Landais, A.: On the limits of climate reconstruction from water stable isotopes in polar ice cores, Past Glob. Chang. Mag., 25, 146–147, https://doi.org/10.22498/pages.25.3.146, 2017.

Casado, M., Landais, A., Picard, G., Münch, T., Laepple, T., Stenni, B., Dreossi, G., Ekaykin, A., Arnaud, L., Genthon, C., and Touzeau, A.: Archival processes of the water stable isotope signal in East Antarctic ice cores, The Cryosphere, 12(5), 1745-1766, https://doi.org/10.5194/tc-12-1745-2018, 2018.

Casado, M., Münch, T., and Laepple, T.: Climatic information archived in ice cores: Impact of intermittency and diffusion on the recorded isotopic signal in Antarctica, Clim. Past, 16, 1581–1598, https://doi.org/10.5194/cp-16-1581-2020, 2020.

Casado, M., Landais, A., Picard, G., Arnaud, L., Dreossi, G., Stenni, B., and Prié, F.: Water Isotopic Signature of Surface Snow Metamorphism in Antarctica, Geophys. Res. Lett., 48, https://doi.org/10.1029/2021GL093382, 2021.

Cauquoin, A., Landais, A., Raisbeck, G. M., Jouzel, J., Bazin, L., Kageyama, M., Peterschmitt, J.-Y., Werner, M., Bard, E., and Team, A.: Comparing past accumulation rate reconstructions in East Antarctic ice cores using ^{10}Be, water isotopes and CMIP5-PMIP3 models, Clim. Past, 11, 355–367, https://doi.org/10.5194/cp-11-355-2015, 2015.

Cauquoin, A., Werner, M., and Lohmann, G.: Water isotopes - Climate relationships for the mid-Holocene and preindustrial period simulated with an isotope-enabled version of MPI-ESM, Clim. Past, 15, 1913–1937, https://doi.org/10.5194/cp-15-1913-2019, 2019.

Cauquoin, A. and Werner, M.: High-Resolution Nudged Isotope Modeling With ECHAM6-Wiso: Impacts of Updated Model Physics and ERA5 Reanalysis Data, J. Adv. Model. Earth Syst., 13, e2021MS002532, https://doi.org/10.1029/2021MS002532, 2021.

Cauquoin, A., Abe-Ouchi, A., Obase, T., Chan, W-L., Paul, A., and Werner, M.: Effects of Last Glacial Maximum (LGM) sea surface temperature and sea ice extent on the isotope–temperature slope at polar ice core sites, Clim. Past, 19, 1275–1294, https://doi.org/10.5194/cp-19-1275-2023, 2023.

Cauquoin, A., and Werner, M.: ECHAM6-wiso and ECHAM5-wiso isotope daily data at Dome Concordia station, East Antarctica [Data set]. Zenodo. https://doi.org/10.5281/zenodo.11468043, 2024.

Connolley, W. M.: The Antarctic temperature inversion, Int. J. Climatol., 16, 1333–1342, https://doi.org/10.1002/(sici)1097-0088(199612)16:12<1333::aid-joc96>3.3.co;2-y, 1996.

Craig, H.: Isotopic variations in meteoric waters, Science, 133, 1702–1703, https://doi.org/10.1126/science.133.3465.1702, 1961.

Crotti, I., Landais, A., Stenni, B., Bazin, L., Parrenin, F., Frezzotti, M., Ritterbusch, F., Lu, Z. T., Jiang, W., Yang, G. M., Fourré, E., Orsi, A., Jacob, R., Minster, B., Prié, F., Dreossi, G., and Barbante, C.: An extension of the TALDICE ice core age scale reaching back to MIS 10.1, Quat. Sci. Rev., 266, 107078, https://doi.org/10.1016/j.quascirev.2021.107078, 2021.

Dansgaard, W.: The Abundance of O^{18} in Atmospheric Water and Water Vapour, Tellus, 5, 461–469, https://doi.org/10.3402/tellusa.v5i4.8697, 1953.

Dansgaard, W.: Stable isotopes in precipitation, Tellus, 16, 436–468, https://doi.org/10.3402/tellusa.v16i4.8993, 1964.

Dansgaard, W., Johnsen, S. J., Møller, J., and Langway, J. R.: One thousand centuries of climatic record from Camp Century on the Greenland ice sheet, Science, 166, 377–381, https://doi.org/10.1126/science.166.3903.377, 1969.

Dansgaard, W., Johnsen, S.J., Clausen, H. B., Dahl-Jensen, D., Gundestrup, N. S., Hammer, C. U., Hvidberg, C. S., Steffensen, J. P., Sveinbjörnsdottir, A. E., Jouzel, J., and Bond, G.: Evidence for general instability of past climate from a 250-kyr ice core record, Nature, 364, 218–220, https://doi.org/10.1038/364218a0, 1993.

Davison, A. C. and Hinkley, D. V.: Bootstrap Methods and Their Applications, Cambridge University Press, Cambridge, UK, ISBN 9780511802843, 1997.

Dee, D. P., Uppala, S. M., Simmons, A. J., Berrisford, P., Poli, P., Kobayashi, S., Andrae, U., Balmaseda, M. A., Balsamo, G., Bauer, P., Bechtold, P., Beljaars, A. C. M., van de Berg, L., Bidlot, J., Bormann, N., Delsol, C., Dragani, R., Fuentes, M., Geer, A.J., Haimberger, L., Healy, S. B., Hersbach, H., Hólm, E. V., Isaksen, L., Kållberg, P., Köhler, M., Matricardi, M., Mcnally, A. P., Monge-Sanz, B. M., Morcrette, J. J., Park, B. K., Peubey, C., de Rosnay, P., Tavolato, C., Thépaut, J. N., and Vitart, F.: The ERA-Interim reanalysis: Configuration and performance of the data assimilation system, Q. J. R. Meteorol. Soc., 137, 553–597, https://doi.org/10.1002/qj.828, 2011.

Delaygue, G., Jouzel, J., Masson, V., Koster, R. D., and Bard, E.: Validity of the isotopic thermometer in central Antarctica: Limited impact of glacial precipitation seasonality and moisture origin, Geophys. Res. Lett., 27, 2677–2680, https://doi.org/10.1029/2000GL011530, 2000.

Delmotte, M., Masson, V., Jouzel, J., and Morgan, V. I.: A seasonal deuterium excess signal at Law Dome, coastal eastern Antarctica: A Southern Ocean signature, J. Geophys. Res. Atmos., 105, 7187–7197, https://doi.org/10.1029/1999JD901085, 2000.

Driemel, A., Augustine, J., Behrens, K., Colle, S., Cox, C., Cuevas-Agulló, E., Denn, F. M., Duprat, T., Fukuda, M., Grobe, H., Haeffelin, M., Hodges, G., Hyett, N., Ijima, O., Kallis, A., Knap, W., Kustov, V., Long, C. N., Longenecker, D., Lupi, A., Maturilli, M., Mimouni, M., Ntsangwane, L., Ogihara, H., Olano, X., Olefs, M., Omori, M., Passamani, L., Pereira, E. B., Schmithüsen, H., Schumacher, S., Sieger, R., Tamlyn, J., Vogt, R., Vuilleumier, L., Xia, X., Ohmura, A., and König-Langlo, G.: Baseline Surface Radiation Network (BSRN): structure and data description (1992–2017), Earth Syst. Sci. Data, 10, 1491-1501, https://doi.org/10.5194/essd-10-1491-2018, 2018.

Ekaykin, A. A., Lipenkov, V. Y., Barkov, N. I., Petit, J. R., and Masson-Delmotte, V.: Spatial and temporal variability in isotope composition of recent snow in the vicinity of Vostok station, Antarctica: implications for ice core record interpretation, Ann. Glaciol., 35, 181–186, https://doi.org/10.3189/172756402781816726, 2002.

Ekaykin, A.A., Lipenkov, V.Y., Kuzmina, I.N., Petit, J.R., Masson-Delmotte, V., and Johnsen, S.J.: The changes in isotope composition and accumulation of snow at Vostok station, East Antarctica, over the past 200 years, Ann. Glaciol., 39, 569–575, https://doi.org/10.3189/172756404781814348, 2004.

Epstein, S. and Mayeda, T.: Variation of O^{18} content of waters from natural sources, Geochim. Cosmochim Acta, 4(5), 213-224, https://doi.org/10.1016/0016-7037(53)90051-9, 1953.

Epstein, S., Sharp, R.P. and Goddard, I.: Oxygen-isotope ratios in Antarctic snow, firn, and ice, J. Geol., 71(6), 698-720, https://doi.org/10.1086/626950, 1963.

EPICA community members: Eight glacial cycles from an Antarctic ice core, Nature, 429, 623–628, https://doi.org/10.1038/nature02599, 2004.

Fogt, R. L. and Marshall, G. J.: The Southern Annular Mode: Variability, trends, and climate impacts across the Southern Hemisphere, Wiley Interdiscip. Rev. Clim. Chang., 11, e652, https://doi.org/10.1002/wcc.652, 2020.

Fox, J. and Weisberg, S.: An R Companion to Applied Regression, 3rd Edition, Sage, Thousand Oaks CA, United States, ISBN 9781544336473, 2018.

Frezzotti, M., Pourchet, M., Flora, O., Gandolfi, S., Gay, M., Urbini, S., Vincent, C., Becagli, S., Gragnani, R., Proposito, M., Severi, M., Traversi, R., Udisti, R., and Fily, M.: New estimations of precipitation and surface sublimation in East Antarctica from snow accumulation measurements, Clim. Dyn., 23, 803–813, https://doi.org/10.1007/s00382-004-0462-5, 2004.

Frezzotti, M., Urbini, S., Proposito, M., Scarchilli, C., and Gandolfi, S.: Spatial and temporal variability of surface mass balance near Talos Dome, East Antarctica, J. Geophys. Res. Earth Surf., 112, F02032, https://doi.org/10.1029/2006JF000638, 2007.

Fujita, K. and Abe, O.: Stable isotopes in Daily precipitation at Dome Fuji, East Antarctica, Geophys. Res. Lett., 33, L18503, https://doi.org/10.1029/2006GL026936, 2006.

Genthon, C., Town, M.S., Six, D., Favier, V., Argentini, S., and Pellegrini, A.: Meteorological atmospheric boundary layer measurements and ECMWF analyses during summer at Dome C, Antarctica, J. Geophys. Res. Atmos., 115, D05104, https://doi.org/10.1029/2009JD012741, 2010.

Genthon, C., Six, D., Gallée, H., Grigioni, P., and Pellegrini, A.: Two years of atmospheric boundary layer observations on a 45-m tower at Dome C on the Antarctic plateau, J. Geophys. Res. Atmos, 118, 3218–3232, https://doi.org/10.1002/jgrd.50128, 2013.

Genthon, C., Six, D., Scarchilli, C., Ciardini, V., and Frezzotti, M.: Meteorological and snow accumulation gradients across Dome C, East Antarctic plateau, Int. J. Climatol., 36, 455–466, https://doi.org/10.1002/joc.4362, 2016.

Genthon, C., Piard, L., Vignon, E., Madeleine, J.-B., Casado, M., and Gallée, H.: Atmospheric moisture supersaturation in the near-surface atmosphere at Dome C, Antarctic Plateau, Atmos. Chem. Phys., 17(1), 691–704, https://doi.org/10.5194/acp-17-691-2017, 2017.

Gonfiantini, R. and Picciotto, E.: Oxygen isotope variations in Antarctic snow samples, Nature, 184, 1557–1558, https://doi.org/10.1038/1841557a0, 1959.

Goursaud, S., Masson-Delmotte, V., Favier, V., Orsi, A., and Werner, M.: Water stable isotope spatio-temporal variability in Antarctica in 1960–2013: Observations and simulations from the ECHAM5-wiso atmospheric general circulation model, Clim. Past, 14(6), 923–946, https://doi.org/10.5194/cp-14-923-2018, 2018.

Grigioni, P., Camporeale, G., Ciardini, V., De Silvestri, L., Iaccarino, A., Proposito, M., and Scarchilli, C.: Dati meteorologici della Stazione meteorologica CONCORDIA presso la Base CONCORDIA STATION (DomeC), ENEA, https://doi.org/10.12910/DATASET2022-002, 2022a.

Grigioni, P., Ciardini, V., Camporeale, G., De Silvestri, L., Iaccarino, A., Proposito, M., and Scarchilli, C.: Dati meteorologici della Stazione di Radiosondaggio presso la Base CONCORDIA STATION (DomeC), ENEA, https://doi.org/10.12910/DATASET2022-004, 2022b.

Groot Zwaaftink, C. D., Cagnati, A., Fierz, C., Macelloni, G., Valt, M., and Lehning, M.: Event-driven deposition of snow on the Antarctic Plateau: Analyzing field measurements with snowpack, Cryosphere, 7(1), 333–347, https://doi.org/10.5194/tc-7-333-2013, 2013.

Hersbach, H., Bell, B., Berrisford, P., Hirahara, S., Horányi, A., Muñoz-Sabater, J., Nicolas, J., Peubey, C., Radu, R., Schepers, D., Simmons, A., Soci, C., Abdalla, S., Abellan, X., Balsamo, G., Bechtold, P., Biavati, G., Bidlot, J., Bonavita, M., De Chiara, G., Dahlgren, P., Dee, D., Diamantakis, M., Dragani, R., Flemming, J., Forbes, R., Fuentes, M., Geer, A., Haimberger, L., Healy, S., Hogan, R.J., Hólm, E., Janisková, M., Keeley, S., Laloyaux, P., Lopez, P., Lupu, C., Radnoti, G., de Rosnay, P., Rozum, I., Vamborg, F., Villaume, S., and Thépaut, J.N.: The ERA5 global reanalysis, Q. J. R. Meteorol. Soc., 146, 1999–2049, https://doi.org/10.1002/qj.3803, 2020.

Hersbach, H., Bell, B., Berrisford, P., Biavati, G., Horányi, A., Muñoz Sabater, J., Nicolas, J., Peubey, C., Radu, R., Rozum, I., Schepers, D., Simmons, A., Soci, C., Dee, D., and Thépaut, J-N.: ERA5 hourly data on single levels from 1940 to present. Copernicus Climate Change Service (C3S) Climate Data Store (CDS), https://doi.org/10.24381/cds.adbb2d47, 2023.

Hoffmann, G., Werner, M., and Heimann, M.: Water isotope module of the ECHAM atmospheric general circulation model: A study on timescales from days to several years, J. Geophys. Res. Atmos., 103, 16871–16896, https://doi.org/10.1029/98JD00423, 1998.

Horita, J.: Hydrogen isotope analysis of natural waters using an H_2-water equilibration method: A special implication to brines, Chemical Geology: Isotope Geoscience Section, 72(1), 89– 94, https://doi.org/10.1016/0168-9622(88)90040-1, 1988.

James, G., Witten, D., Hastie, T., and Tibshirani, R.: An introduction to Statistical Learning with Applications in R, Springer, New York, NY, USA, ISBN 9781461471387, https://doi.org/10.1007/978-1-4614-7138-7, 2013.

Joussaume, S., Sadourny, R., and Jouzel, J.: A general circulation model of water isotope cycles in the atmosphere, Nature, 311, 24–29, https://doi.org/10.1038/311024a0, 1984.

Jouzel, J.: Water stable isotopes: Atmospheric composition and applications in polar ice core studies, in: Treatise on Geochemistry, 2nd Edition., Vol. 5, The Atmosphere, edited by: Keeling, R. and Russel, L., Elsevier, Amsterdam, The Netherlands, 213–256, https://doi.org/10.1016/B978-0-08-095975-7.00408-3, 2014.

Jouzel, J. and Merlivat, L.: Deuterium and oxygen 18 in precipitation: Modeling of the isotopic effects during snow formation, J. Geophys. Res., 89, 11749–11757, https://doi.org/10.1029/JD089iD07p11749, 1984.

Jouzel, J., Russell, G. L., Suozzo, R. J., Koster, D., White, J. W. C., and Broecker, W. S.: Simulations of the HDO and $H_2{}^{18}O$ atmospheric cycles using the NASA GISS general circulation model: The seasonal cycle for present-day conditions, J. Geophys. Res., 92, 14739–14760, https://doi.org/10.1029/JD092iD12p14739, 1987.

Jouzel, J., Alley, R. B., Cuffey, K. M., Dansgaard, W., Grootes, P., Hoffmann, G., Johnsen, S. J., Koster, R. D., Peel, D., Shuman, C. A., Stievenard, M., Stuiver, M., and White, J.: Validity of the temperature reconstruction from water isotopes in ice cores, J. Geophys. Res., 102, 26471–26487, https://doi.org/10.1029/97JC01283, 1997.

Jouzel, J., Vimeux, F., Caillon, N., Delaygue, G., Hoffmann, G., Masson-Delmotte, V., and Parrenin, F.: Magnitude of isotope/temperature scaling for interpretation of central Antarctic ice cores, J. Geophys. Res., 108, 4361, https://doi.org/10.1029/2002JD002677, 2003.

Jouzel, J., Masson-Delmotte, V., Cattani, O., Dreyfus, G., Falourd, S., Hoffmann, G., Minster, B., Nouet, J., Barnola, J. M., Chappellaz, J., Fisher, H., Gallet, J. C., Johnsen, S., Leuenberger, M., Loulergue, L., Luethi, D., Oerter, H., Parrenin, F., Raisbeck, G., Raynaud, D., Schilt, A., Schwander, J., Selmo, E., Souchez, R., Spahni, R., Stauffer, B., Steffensen, J. P., Stenni, B., Stocker, T. F., Tison, J. L., Werner, M., and Wolff, E. W.: Orbital and millennial Antarctic climate variability over the past 800,000 years, Science, 317, 793–796, https://doi.org/10.1126/science.1141038, 2007.

Kawamura, K., Abe-Ouchi, A., Motoyama, H., Ageta, Y., Aoki, S., Azuma, N., Fujii, Y., Fujita, K., Fujita, S., Fukui, K., Furukawa, T., Furusaki, A., Goto-Azuma, K., Greve, R., Hirabayashi, M., Hondoh, T., Hori, A., Horikawa, S., Horiuchi, K., Igarashi, M., Iizuka, Y., Kameda, T., Kanda, H., Kohno, M., Kuramoto, T., Matsushi, Y., Miyahara, M., Miyake, T., Miyamoto, A., Nagashima, Y., Nakayama, Y., Nakazawa, T., Nakazawa, F., Nishio, F., Obinata, I., Ohgaito, R., Oka, A., Okuno, J., Okuyama, J., Oyabu, I., Parrenin, F., Pattyn, F., Saito, F., Saito, Takashi, Saito, Takeshi, Sakurai, T., Sasa, K., Seddik, H., Shibata, Y., Shinbori, K., Suzuki, K., Suzuki, T., Takahashi, A., Takahashi, K., Takahashi, S., Takata, M., Tanaka, Y., Uemura, R., Watanabe, G., Watanabe, O., Yamasaki, T., Yokoyama, K., Yoshimori, M., and Yoshimoto, T.: State dependence of climatic instability over the past 720,000 years from Antarctic ice cores and climate modeling, Sci. Adv., 3, e1600446, https://doi.org/10.1126/sciadv.1600446, 2017.

Kendall, T.: Rank Correlation Methods, 4th ed., Charles Griffin, London, UK, 1975.

Krinner, G., Genthon, C., and Jouzel, J.: GCM analysis of local influences on ice core delta signals, Geophys. Res. Lett., 24, 2825–2828, https://doi.org/10.1029/97gl52891, 1997.

Kuhn, M.: caret: Classification and Regression Training. R package version 6.0-93, https://CRAN.R-project.org/package=caret, 2022.

Laepple, T., Münch, T., Casado, M., Hoerhold, M., Landais, A., and Kipfstuhl, S.: On the similarity and apparent cycles of isotopic variations in East Antarctic snow pits, Cryosphere, 12, 169–187, https://doi.org/10.5194/tc-12-169-2018, 2018.

Langway, C. C.: A 400 Meter Deep Ice Core in Greenland: Preliminary Report, J. Glaciol., 3, 217–217, https://doi.org/10.3189/s0022143000024278, 1958.

Leisch, F.: Bootstrap: Functions for the Book “An Introduction to the Bootstrap”, R package version 2019.6, https://CRAN.R-project.org/package=bootstrap, 2019.

Lupi, A., Lanconelli, C., and Vitale, V.: Basic and other measurements of radiation at Concordia station (2006-01 et seq), Institute of Atmospheric Sciences and Climate of the Italian National Research Council, Bologna, PANGAEA, https://doi.org/10.1594/PANGAEA.935421, 2021.

Ma, T., Li, L., Shi, G., Li, Y.: Acquisition of post-depositional effects on stable isotopes (δ18O and δD) of snow and firn at Dome A, East Antarctica, Water (Switzerland), 12, 1707, https://doi.org/10.3390/W12061707, 2020.

Maindonald, J. and Braun, J. W.: Data Analysis and Graphics Using R, Third Edition. Cambridge University Press, Cambridge, UK, 565 pp., ISBN 9780511712869, 2011.

Mangiafico, S.: rcompanion: Functions to Support Extension Education Program Evaluation, R package version 2.4.18, https://CRAN.R-project.org/package=rcompanion, 2022.

Mann, H. B.: Nonparametric Tests Against Trend. Econometrica 13, 245, https://doi.org/10.2307/1907187, 1945.

Marshall G. J.: Trends in the Southern Annular Mode from Observations and Reanalyses, J. Clim., 16, 4134–4143, https://doi.org/10.1175/1520-0442(2003)016%3C4134:TITSAM%3E2.0.CO;2, 2003.

Masson-Delmotte, V., Hou, S., Ekaykin, A., Jouzel, J., Aristarain, A., Bernardo, R.T., Bromwich, D., Cattani, O., Delmotte, M.M., Falourd, S., Frezzotti, M., Gallée, H., Genoni, L., Isaksson, E., Landais, A., Helsen, M.M., Hoffmann, G., Lopez, J., Morgan, V., Motoyama, H., Noone, D., Oerter, H., Petit, J. R., Royer, A., Uemura, R., Schmidt, G. A., Schlosser, E., Simões, J. C., Steig, E. J., Stenni, B., Stievenard, M., Van Den Broeke, M. R., Van De Wal, R. S. W., Van De Berg, W. J., Vimeux, F., and White, J. W. C.: A review of antarctic surface snow isotopic composition: Observations, atmospheric circulation, and isotopic modeling, J. Clim., 21, 3359–3387, https://doi.org/10.1175/2007JCLI2139.1, 2008.

Mathieu, R., Pollard, D., Cole, J. E., White, J. W. C., Webb, R. S., and Thompson, S. L.: Simulation of stable water isotope variations by the GENESIS GCM for modern conditions, J. Geophys. Res., 107, 4037, https://doi.org/10.1029/2001JD900255, 2002.

Merlivat, L. and Jouzel J.: Global climatic interpretation of the deuterium-oxygen 18 relationship for precipitation, J. Geophys. Res., 84, 5029–5033, https://doi.org/10.1029/JC084iC08p05029, 1979.

Mo, K. C.: Relationships between low-frequency variability in the Southern Hemisphere and sea surface temperature anomalies, J. Clim., 13, 3599–3610, https://doi.org/10.1175/1520-0442(2000)013<3599:RBLFVI>2.0.CO;2, 2000.

Münch, T., Kipfstuhl, S., Freitag, J., Meyer, H., and Laepple, T.: Regional climate signal vs. local noise: a twodimensional view of water isotopes in Antarctic firn at Kohnen Station, Dronning Maud Land, Clim. Past, 12, 1565-1581, https://doi.org/10.5194/cp-12-1565-2016, 2016.

Münch, T., Laepple, T.: What climate signal is contained in decadal - To centennial-scale isotope variations from Antarctic ice cores?, Clim. Past ,14, 2053–2070, https://doi.org/10.5194/cp-14-2053-2018, 2018.

Murphy, D.M. and Koop, T.: Review of the vapour pressures of ice and supercooled water for atmospheric applications, Quart. J. Royal Met. Soc, 131(608), 1539-1565, https://doi.org/10.1256/qj.04.94, 2005.

Nusbaumer, J., Wong, T. E., Bardeen, C., and Noone, D.: Evaluating hydrological processes in the Community Atmosphere Model Version 5 (CAM5) using stable isotope ratios of water, J. Adv. Model. Earth Sy., 9, 949–977, https://doi.org/10.1002/2016ms000839, 2017.

Ohmura, A., Dutton, E. G., Forgan, B., Frohlich, C., Gilgen, H., Hegner, H., Heimo, A., König-Langlo, G., McArthur, B., Muller, G., Philipona, R., Pinker, R., Whitlock C. H., Dehne K., and Wild, M.: Baseline Surface Radiation Network (BSRN/WCRP): New Precision Radiometry for Climate Research, Bull. Amer. Meteor. Soc., 79, 2115–2136, https://doi.org/10.1175/1520-0477(1998)079%3C2115:BSRNBW%3E2.0.CO;2, 1998.

Okazaki, A., and Yoshimura, K.: Global evaluation of proxy system models for stable water isotopes with realistic atmospheric forcing, J. Geophys. Res. Atmos., 124, 8972–8993, https://doi.org/10.1029/2018JD029463, 2019.

Palerme, C., Genthon, C., Claud, C., Kay, J.E., Wood, N.B., and L'Ecuyer, T.: Evaluation of current and projected Antarctic precipitation in CMIP5 models, Clim. Dyn., 48, 225–239, https://doi.org/10.1007/s00382-016-3071-1, 2017

Parrenin, F., Fujita, S., Abe-Ouchi, A., Kawamura, K., Masson-Delmotte, V., Motoyama, H., Saito, F., Severi, M., Stenni, B., Uemura, R., and Wolff, E. W.: Climate dependent contrast in surface mass balance in East Antarctica over the past 216 ka, J. Glaciol., 62, 1037–1048, https://doi.org/10.1017/jog.2016.85, 2016.

Parrenin, F., Cavitte, M. G. P., Blankenship, D. D., Chappellaz, J., Fischer, H., Gagliardini, O., Masson-Delmotte, V., Passalacqua, O., Ritz, C., Roberts, J., Siegert, M. J., and Young, D. A.: Is there 1.5-million-year-old ice near Dome C, Antarctica?, Cryosphere, 11, 2427–2437, https://doi.org/10.5194/tc-11-2427-2017, 2017.

Penna, D., Stenni, B., Šanda, M., Wrede, S., Bogaard, T.A., Michelini, M., Fischer, B. M. C., Gobbi, A., Mantese, N., Zuecco, G., Borga, M., Bonazza, M., Sobotková, M., Čejková, B., and Wassenaar, L. I.: Technical note: Evaluation of between-sample memory effects in the analysis of δ^2H and $\delta^{18}O$ of water samples measured by laser spectroscopes, Hydrol. Earth Syst. Sci., 16, 3925–3933, https://doi.org/10.5194/hess-16-3925-2012, 2012

Petenko, I., Argentini, S., Casasanta, G., Genthon, C., and Kallistratova, M.: Stable Surface-Based Turbulent Layer During the Polar Winter at Dome C, Antarctica: Sodar and In Situ Observations, Boundary-Layer Meteorol., 171, 101–128, https://doi.org/10.1007/s10546-018-0419-6, 2019.

Petit, J. R., Jouzel, J., Pourchet, M., and Merlivat, L.: A detailed study of snow accumulation and stable isotope content in Dome C (Antarctica), J. Geophys. Res.-Oceans, 87, 4301–4308, https://doi.org/10.1029/JC087iC06p04301, 1982.

Petit, J.R., Jouzel, J., Raynaud, D., Barkov, N. I., Barnola, J. M., Basile, I., Bender, M., Chappellaz, J., Davis, M., Delaygue, G., Delmotte, M., Kotiyakov, V.M., Legrand, M., Lipenkov, V.Y., Lorius, C., Pépin, L., Ritz, C., Saltzman, E., and Stievenard, M.: Climate and atmospheric history of the past 420,000 years from the Vostok ice core, Antarctica, Nature, 399, 429–436, https://doi.org/10.1038/20859, 1999.

Pfahl, S. and Sodemann, H.: What controls deuterium excess in global precipitation?, Clim. Past, 10, 771–781, https://doi.org/10.5194/cp-10-771-2014, 2014.

Picard, G., Domine, F., Krinner, G., Arnaud, L., and Lefebvre, E.: Inhibition of the positive snow-albedo feedback by precipitation in interior Antarctica, Nature Clim. Chang., 2(11), 795–798, https://doi.org/10.1038/nclimate1590, 2012.

Picard, G., Arnaud, L., Caneill, R., Lefebvre, E., and Lamare, M.: Observation of the process of snow accumulation on the Antarctic Plateau by time lapse laser scanning, Cryosphere, 13(7), 1983–1999, https://doi.org/10.5194/tc-13-1983-2019, 2019.

Pierce, D.: ncdf4: Interface to unidata netCDF (version 4 or earlier) format data files, R package version 1.21, https://CRAN.R-project.org/package=ncdf4, 2023

Pietroni, I., Argentini, S., and Petenko, I.: One Year of Surface-Based Temperature Inversions at Dome C, Antarctica, Boundary-Layer Meteorol., 150, 131–151, https://doi.org/10.1007/s10546-013-9861-7, 2014.

R Core Team: R: A language and environment for statistical computing, R Foundation for Statistical Computing, Vienna, Austria, https://www.R-project.org/, 2022.

Risi, C., Bony, S., Vimeux, F., and Jouzel, J.: Water-stable isotopes in the LMDZ4 general circulation model: Model evaluation for present-day and past climates and applications to climatic interpretations of tropical isotopic records, J. Geophys. Res. Atmos., 115, D12118, https://doi.org/10.1029/2009JD013255, 2010.

Ritter, F., Christian Steen-Larsen, H., Werner, M., Masson-Delmotte, V., Orsi, A., Behrens, M., Birnbaum, G., Freitag, J., Risi, C., and Kipfstuhl, S.: Isotopic exchange on the diurnal scale between near-surface snow and lower atmospheric water vapor at Kohnen station, East Antarctica, Cryosphere, 10, 1647–1663, https://doi.org/10.5194/tc-10-1647-2016, 2016.

Roeckner, E., Baeuml, G., Bonaventura, L., Brokopf, R., Esch, M., Giorgetta, M., Hagemann, S., Kirchner, I., Kornblueh, L., Manzini, E., Rhodin, A., Schlese, U., Schulzweida, U., and Tompkins, A.: The general circulation model ECHAM5. Part I: Model description, MPI-Report, https://mpimet.mpg.de/fileadmin/models/echam/mpi_report_349.pdf, 2003.

Rozanski, K., Araguás-Araguás, L., and Gonfiantini, R.: Isotopic Patterns in Modern Global Precipitation, Clim. Chang. Cont. Isot. Rec. Geophys. Monogr. Ser., vol. 78, https://doi.org/10.1029/gm078p0001, 1993.

Scarchilli, C., Frezzotti, M., Grigioni, P., De Silvestri, L., Agnoletto, L., and Dolci, S.: Extraordinary blowing snow transport events in East Antarctica, Clim. Dyn., 34, 1195–1206, https://doi.org/10.1007/s00382-009-0601-0, 2010.

Scarchilli, C., Frezzotti, M., and Ruti, P. M.: Snow precipitation at four ice core sites in East Antarctica: Provenance, seasonality and blocking factors, Clim. Dyn., 37, 2107–2125, https://doi.org/10.1007/s00382-010-0946-4, 2011.

Schlosser, E., Reijmer, C., Oerter, H., and Graf, W.: The influence of precipitation origin on the δ18O-T relationship at Neumayer station, Ekströmisen, Antarctica, Ann. Glaciol., 39, 41–48, https://doi.org/10.3189/172756404781814276, 2004.

Schlosser, E., Oerter, H., Masson-Delmotte, V., and Reijmer, C. Atmospheric influence on the deuterium excess signal in polar firn: Implication for ice-core interpretation, J. Glaciol., 54, 117–124, https://doi.org/10.3189/002214308784408991, 2008.

Schmidt, G. A., G. Hoffmann, D. T. Shindell, and Hu Y.: Modelling atmospheric stable water isotopes and the potential for constraining cloud processes and stratosphere-troposphere water exchange, J. Geophys. Res., 110, D21314, https://doi:10.1029/2005JD005790, 2005.

Sen, P. K.: Estimates of the Regression Coefficient Based on Kendall's Tau, J. Am. Stat. Assoc., 63, 1379–1389, https://doi.org/10.1080/01621459.1968.10480934, 1968.

Servettaz, A. P. M., Agosta, C., Kittel, C., and Orsi, A. J.: Control of the temperature signal in Antarctic proxies by snowfall dynamics, Cryosphere, 17, 5373–5389, https://doi.org/10.5194/tc-17-5373-2023, 2023.

Sime, L., Wolff, E., Oliver, K., and Tindall, J.C.: Evidence for warmer interglacials in East Antarctic ice cores, Nature, 462, 342–345, https://doi.org/10.1038/nature08564, 2009.

Stenni, B., Scarchilli, C., Masson-Delmotte, V., Schlosser, E., Ciardini, V., Dreossi, G., Grigioni, P., Bonazza, M., Cagnati, A., Karlicek, D., Risi, C., Udisti, R., and Valt, M.: Three-year monitoring of stable isotopes of precipitation at Concordia Station, East Antarctica, Cryosphere, 10, 2415–2428, https://doi.org/10.5194/tc-10-2415-2016, 2016.

Stenni, B., Curran, M. A. J., Abram, N. J., Orsi, A., Goursaud, S., Masson-Delmotte, V., Neukom, R., Goosse, H., Divine, D., Van Ommen, T., Steig, E. J., Dixon, D. A., Thomas, E. R., Bertler, N. A. N., Isaksson, E., Ekaykin, A., Werner, M., and Frezzotti, M.: Antarctic climate variability on regional and continental scales over the last 2000 years, Clim. Past, 13, 1609–1634, https://doi.org/10.5194/cp-13-1609-2017, 2017.

Stevens, B., Giorgetta, M., Esch, M., Mauritsen, T., Crueger, T., Rast, S., Salzmann, M., Schmidt, H., Bader, J., Block, K., Brokopf, R., Fast, I., Kinne, S., Kornblueh, L., Lohmann, U., Pincus, R., Reichler, T., Roeckner, E.: Atmospheric component of the MPI-M earth system model: ECHAM6, J. Adv. Model. Earth Syst., 5, 146–172, https://doi.org/10.1002/jame.20015, 2013.

Theil, H.: A Rank-Invariant Method of Linear and Polynomial Regression Analysis, Proc. R. Netherlands Acad. Sci., 53, 386–392, https://doi.org/10.1007/978-94-011-2546-8_20, 1950.

Thompson, D. and Wallace, J.: Annular Modes in the Extratropical Circulation. Part I: Month-to-Month Variability, J. Clim., 13, 1000–1016, https://doi.org/10.1175/1520-0442(2000)013%3C1000:AMITEC%3E2.0.CO;2, 2000.

Touzeau, A., Landais, A., Stenni, B., Uemura, R., Fukui, K., Fujita, S., Guilbaud, S., Ekaykin, A., Casado, M., Barkan, E., Luz, B., Magand, O., Teste, G., Le Meur, E., Baroni, M., Savarino, J., Bourgeois, I., and Risi, C.: Acquisition of isotopic composition for surface snow in East Antarctica and the links to climatic parameters, Cryosphere, 10, 837–852, https://doi.org/10.5194/tc-10-837-2016, 2016.

Turner, J., Phillips, T., Thamban, M., Rahaman, W., Marshall, G. J., Wille, J. D., Favier, V., Winton, V. H. L., Thomas, E., Wang, Z., van den Broeke, M., Hosking, J. S., and Lachlan-Cope, T.: The Dominant Role of Extreme Precipitation Events in Antarctic Snowfall Variability, Geophys. Res. Lett., 46, 3502–3511, https://doi.org/10.1029/2018GL081517, 2019.

Uemura, R., Matsui, Y., Yoshimura, K., Motoyama, H., and Yoshida, N.: Evidence of deuterium excess in water vapor as an indicator of ocean surface conditions, J. Geophys. Res. Atmos., 113, D19114, https://doi.org/10.1029/2008JD010209, 2008.

Uemura, R., Masson-Delmotte, V., Jouzel, J., Landais, A., Motoyama, H., and Stenni, B.: Ranges of moisture-source temperature estimated from Antarctic ice cores stable isotope records over glacial-interglacial cycles, Clim. Past, 8, 1109–1125, https://doi.org/10.5194/cp-8-1109-2012, 2012.

Urbini, S., Frezzotti, M., Gandolfi, S., Vincent, C., Scarchilli, C., Vittuari, L., and Fily, M.: Historical behaviour of Dome C and Talos Dome (East Antarctica) as investigated by snow accumulation and ice velocity measurements, Glob. Planet. Change, 60, 576–588, https://doi.org/10.1016/j.gloplacha.2007.08.002, 2008.

Vimeux, F., Masson, V., Jouzel, J., Stievenard, M., Petit, J. R.: Glacial-interglacial changes in ocean surface conditions in the Southern Hemisphere, Nature, 398, 410–413, https://doi.org/10.1038/18860, 1999.

Wei, T. and Simko, V.: R package "corrplot": Visualization of a Correlation Matrix, (Version 0.92), https://Github.Com/Taiyun/Corrplot, 2021.

Werner, M., Langebroek, P.M., Carlsen, T., Herold, M., and Lohmann, G.: Stable water isotopes in the ECHAM5 general circulation model: Toward high-resolution isotope modeling on a global scale, J. Geophys. Res. Atmos., 116, D15109, https://doi.org/10.1029/2011JD015681, 2011.

Wood, S.N.: Generalized Additive Models: An Introduction with R (2nd edition), Chapman and Hall/CRC, 496 pp., ISBN 9781315370279, https://doi.org/10.1201/9781315370279, 2017.

Yoshimura, K.: Stable Water Isotopes in Climatology, Meteorology, and Hydrology: A Review. Journal of the Meteorological Society of Japan, Ser. II, 2015, Volume 93, Issue 5, 513-533, https://doi.org/10.2151/jmsj.2015-036, 2015.

Zannoni, D., Steen-Larsen, H. C., Peters, A.J., Wahl, S., Sodemann, H., and Sveinbjörnsdóttir, A. E.: Non-Equilibrium Fractionation Factors for D/H and $^{18}O/^{16}O$ During Oceanic Evaporation in the North-West Atlantic Region, J. Geophys. Res. Atmos, 127, e2022JD037076, https://doi.org/10.1029/2022JD037076, 2022.

Zeileis, A. and Grothendieck, G.: Zoo: S3 infrastructure for regular and irregular time series, J. Stat. Softw., 14, https://doi.org/10.18637/jss.v014.i06, 2005.